

# The SEGUE Stellar Parameter Pipeline. V. Estimation of Alpha-Element Abundance Ratios From Low-Resolution SDSS/SEGUE Stellar Spectra

Young Sun Lee<sup>1</sup>, Timothy C. Beers<sup>1</sup>, Carlos Allende Prieto<sup>2,3,4</sup>, David K. Lai<sup>5</sup>, Constance M. Rockosi<sup>5</sup>, Heather L. Morrison<sup>6</sup>, Jennifer A. Johnson<sup>7</sup>, Deokkeun An<sup>8</sup>, Thirupathi Sivarani<sup>9</sup>, Brian Yanny<sup>10</sup>

## ABSTRACT

We present a method for the determination of  $[\alpha/\text{Fe}]$  ratios from low-resolution ( $R = 2000$ ) SDSS/SEGUE stellar spectra. By means of a star-by-star comparison with degraded spectra from the ELODIE spectral library and with a set of moderately high-resolution ( $R = 15,000$ ) and medium-resolution ( $R = 6000$ ) spectra of SDSS/SEGUE stars, we demonstrate that we are able to measure  $[\alpha/\text{Fe}]$  from SDSS/SEGUE spectra (with  $S/N > 20/1$ ) to a precision of better than 0.1 dex, for stars with atmospheric parameters in the range  $T_{\text{eff}} = [4500, 7000]$  K,  $\log g = [1.5, 5.0]$ , and  $[\text{Fe}/\text{H}] = [-1.4, +0.3]$ , over the range  $[\alpha/\text{Fe}] = [-0.1, +0.6]$ . For stars with  $[\text{Fe}/\text{H}] < -1.4$ , our method requires spectra with slightly higher signal-to-noise to achieve this precision ( $S/N > 25/1$ ). Over the full temperature range considered, the lowest metallicity star for which a confident estimate of  $[\alpha/\text{Fe}]$  can be obtained from our approach is  $[\text{Fe}/\text{H}]$

---

<sup>1</sup>Department of Physics and Astronomy and JINA (Joint Institute for Nuclear Astrophysics), Michigan State University, East Lansing, MI 48824, USA; lee@pa.msu.edu, beers@pa.msu.edu

<sup>2</sup>Instituto de Astrofísica de Canarias, E-38205 La Laguna, Tenerife, Spain

<sup>3</sup>Departamento de Astrofísica, Universidad de La Laguna, E-38206 La Laguna, Tenerife, Spain

<sup>4</sup>Mullard Space Science Laboratory, University College London, Holmbury St. Mary, Dorking, RH5 6NT Surrey, UK; cap@mssl.ucl.ac.uk

<sup>5</sup>UCO/Lick Observatory, Department of Astronomy and Astrophysics, University of California, Santa Cruz, CA 95064, USA; david@ucolick.org, crockosi@ucolick.org

<sup>6</sup>Department of Astronomy, Case Western Reserve University, Cleveland, OH 44106, USA; heather@vegemite.case.edu

<sup>7</sup>Department of Astronomy, Ohio State University, Columbus, OH 43210, USA; jaj@astronomy.ohio-state.edu

<sup>8</sup>Department of Science Education, Ewha Womans University, Seoul 120-750, Republic of Korea; deokkeun@ewha.ac.kr

<sup>9</sup>Indian Institute of Astrophysics, 2nd block Koramangala, Bangalore 560034, India; sivarani@iiap.res.in

<sup>10</sup>Fermi National Accelerator Laboratory, Batavia, IL 60510, USA; yanny@fnal.gov

$\sim -2.5$ ; preliminary tests indicate that a metallicity limit as low as  $[\text{Fe}/\text{H}] \sim -3.0$  may apply to cooler stars. As a further validation of this approach, weighted averages of  $[\alpha/\text{Fe}]$  obtained for SEGUE spectra of likely member stars of Galactic globular clusters (M15, M13, and M71) and open clusters (NGC 2420, M67, and NGC 6791) exhibit good agreement with the values of  $[\alpha/\text{Fe}]$  from previous studies. The results of the comparison with NGC 6791 imply that the metallicity range for the method may extend to  $\sim +0.5$ .

*Subject headings:* methods: data analysis — stars: abundances, fundamental parameters — surveys — techniques: imaging spectroscopy

## 1. Introduction

The chemical elements O, Mg, Si, Ca, and Ti, which are often referred to as the “ $\alpha$ ” elements, are mainly produced in the interiors of high-mass stars ( $> 8 M_{\odot}$ ) during their main-sequence lifetime and later explosive nucleosynthesis events. These elements, at least some fraction of which are ejected into the interstellar medium (ISM) by core-collapse supernovae (Timmes et al. 1995), enhance the next generations of stars that form out of this polluted ISM. The abundances of the  $\alpha$ -elements for subsequent stellar generations thus increase very quickly, due to the relatively short main-sequence lifetimes of massive stars (millions to tens of millions of years). However, as Fe can be produced by the same process, enhancements of the  $[\alpha/\text{Fe}]$ <sup>11</sup> ratios remain at roughly the same levels. Substantially more Fe is generated by Type Ia supernovae (SNe Ia), whose progenitor lifetimes are much longer (on the order of 0.1 Gyr to a few Gyr; Matteucci & Recchi 2001). Nucleosynthesis during these explosions is thought to produce a large fraction of the iron-peak elements (Ni, Co, Fe, etc.; Nomoto et al. 1984). Hence, an ISM polluted by material enriched with these iron-peak elements at later times will naturally lead to stars that form with relatively low  $[\alpha/\text{Fe}]$  ratios.

In the Milky Way, a typical metal-poor halo star exhibits abundance ratios  $[\alpha/\text{Fe}] \sim +0.4$  (e.g., McWilliam 1997). Thick-disk stars have relatively higher abundance ratios ( $[\alpha/\text{Fe}] \sim +0.3$  to  $+0.4$ ; Bensby et al. 2003, 2005; Reddy et al. 2006) than do thin-disk stars ( $[\alpha/\text{Fe}] \sim 0.0$  to  $+0.1$ ). Many stars in the dwarf spheroidal galaxies (dSphs) in the vicinity of the Milky Way possess relatively lower  $[\alpha/\text{Fe}]$  compared to the Galactic halo stars of the same metallicity (Shetrone et al. 2001, 2003; Fulbright 2002; Tolstoy et al. 2003; Geisler et al. 2005), at least for  $[\text{Fe}/\text{H}] > -2.5$ . It

---

<sup>11</sup>This notation is defined by an average of  $[\text{Mg}/\text{Fe}]$ ,  $[\text{Si}/\text{Fe}]$ ,  $[\text{Ca}/\text{Fe}]$ , and  $[\text{Ti}/\text{Fe}]$  in many works, and it is similarly applied in this paper.

is thought that the low  $[\alpha/\text{Fe}]$  ratio in these systems is due to a more inefficient star formation history, resulting in a greater contribution of Fe from SNe Ia than occurred for the bulk of the halo stars of the Milky Way (Unavane et al. 1996). Recent evidence has been accumulating (e.g., Frebel et al. 2010, and references therein) that the  $[\alpha/\text{Fe}]$  ratios for the lowest metallicity stars in dSphs (including the majority of stars in the low-luminosity dSphs discovered by the Sloan Digital Sky Survey (SDSS; Zucker et al. 2006a, 2006b; Belokurov et al. 2006, 2007, 2008, 2010) are quite similar to those observed for stars in the Galactic halo with  $[\text{Fe}/\text{H}] < -2.5$ , strengthening the argument of Carollo et al. (2007, 2010) and Frebel et al. (2010) that dSphs may well have contributed to (at least) the formation of the outer-halo component of the Galaxy.

As the evolution of chemical abundances in a given system is closely related to the history of its star formation (e.g., Tinsley 1979), abundance ratios such as  $[\alpha/\text{Fe}]$  can be used to explore these histories for recognized components of the Galaxy and its satellites, in particular if such measurements can be obtained for large numbers of member stars.

Past efforts to measure the abundance of  $\alpha$ -elements have been mostly based on high signal-to-noise ratio (S/N), high-resolution ( $R > 20,000$ ) spectroscopy, since individual elemental lines can be identified relatively easily and used to obtain the most accurate abundances. However, with current generation telescopes and instrumentation, the (typically) long exposure times required generally limit the samples of targets to bright stars or small numbers of fainter stars, and it is not (yet) feasible to obtain high-resolution spectra for the large numbers of stars needed to systematically study the history of star formation and chemical enrichment of the recognized Galactic components.

The above limitations have inspired investigations of techniques capable of recovering estimates of abundances for  $\alpha$ -elements using lower resolution spectroscopy. For example, Kirby et al. (2008a) developed a spectral matching technique based on medium-resolution ( $R \sim 6000$ ) spectra over the wavelength range 6300 – 9100 Å. This approach simultaneously measures  $[\text{Fe}/\text{H}]$  and  $[\alpha/\text{Fe}]$ , and has been validated by comparing the derived atmospheric parameters with giants in seven Galactic globular clusters (GCs) over a range of metallicity. The basic idea of the method is to generate a grid of synthetic spectra spanning various temperature, gravity, and metallicity ranges having different  $\alpha$ -abundances, and search this grid for the best-matching synthetic spectrum to a given observed spectrum. The parameters of the best-matching synthetic spectrum (i.e., the global minimum of  $\chi^2$ ) are then adopted. In their approach, Kirby et al. chose to fix  $T_{\text{eff}}$  and  $\log g$  based on measured photometry (and extrapolation of known relationships between  $T_{\text{eff}}$  and  $\log g$  for giant-branch stars). They report a precision for the determination of  $[\text{Fe}/\text{H}]$  of about 0.1 dex, and as low as 0.05 dex for  $[\alpha/\text{Fe}]$  for high-S/N spectra. They then applied this technique to derive  $[\text{Fe}/\text{H}]$  for red giants in low-luminosity dSphs (Kirby et al. 2008b), and similarly, to velocity-member stars in the classical Sculptor dwarf galaxy (Kirby et al. 2009), and were able to estimate  $[\text{Fe}/\text{H}]$  and the

abundances of Mg, Si, Ca, and Ti for stars in their sample of dwarf galaxies.

As another example, one contemporary survey that obtains abundances of the  $\alpha$ -elements for large samples of stars is the Radial Velocity Experiment (RAVE; Steinmetz et al. 2006), a spectroscopic survey for (up to) a million stars in the southern sky. The spectral range explored is 8410 – 8795 Å, at a resolving power  $R = 7500$ . Using an extensive grid of synthetic spectra and a penalized  $\chi^2$  matching technique, reasonably accurate estimates of  $T_{\text{eff}}$ ,  $\log g$ , [Fe/H], and somewhat less accurate  $[\alpha/\text{Fe}]$  are obtained for the observed stars (Second Data Release; Zwitter et al. 2008). RAVE is limited to bright stars ( $9 < I < 12$ ), so that the information gathered will be most useful for exploration of the thin- and thick-disk populations.

The Sloan Extension for Galactic Understanding and Exploration (SEGUE; Yanny et al. 2009) was one of three surveys that were executed as part of the extension of the SDSS-II, which comprised the sub-surveys Legacy, Supernova Survey, and SEGUE. The SEGUE program was designed, in part, to obtain *ugriz* imaging of some 3500 deg<sup>2</sup> of sky outside of the original SDSS-I footprint (Fukugita et al. 1996; Gunn et al. 1998, 2006; York et al. 2000; Stoughton et al. 2002; Abazajian et al. 2003, 2004, 2005, 2009; Pier et al. 2003; Adelman-McCarthy et al. 2006, 2007, 2008), and roughly 240,000 low-resolution ( $R = 2000$ ) stellar spectra covering the wavelength range 3820 – 9100 Å. A one year dedicated survey devoted to obtaining such spectra for fainter stars, SEGUE-II, executed as part of the ongoing SDSS-III extension, has added an additional  $\sim 140,000$  stars. Stellar spectra obtained during regular SDSS-I and SDSS-II operation add roughly another 100,000 stars, for a total of about 500,000 stars with potentially suitable spectra for further analysis.

These SDSS/SEGUE stellar spectra are processed through the SEGUE Stellar Parameter Pipeline (SSPP; Lee et al. 2008a, 2008b, Allende Prieto et al. 2008, Smolinski et al. 2010; Paper I, Paper II, Paper III, Paper IV respectively, hereafter), and the three primary stellar parameters ( $T_{\text{eff}}$ ,  $\log g$ , and [Fe/H]) are reported for most stars in the temperature range 4000 – 10,000 K and with spectral S/N ratios exceeding 10/1 (averaged over the entire spectrum). The SSPP estimates the atmospheric parameters via application of a number of approaches, such as a minimum distance method (Allende Prieto et al. 2006), neural network analysis (Bailer-Jones 2000; Willemsen et al. 2005; Re Fiorentin et al. 2007), auto-correlation analysis (Beers et al. 1999), and a variety of line index calculations based on previous calibrations with respect to known standard stars (Beers et al. 1999; Cenarro et al. 2001a,b; Morrison et al. 2003). The SSPP adopts 6 primary methods for estimation of  $T_{\text{eff}}$ , 10 for  $\log g$ , and 12 for [Fe/H]. A series of additional procedures are used, especially for [Fe/H], to obtain refined estimates of the final averages of the multiple determinations for each parameter. We refer the interested reader to Paper I for more details on the SSPP. Paper I also performs a preliminary comparison with an average of two different high-resolution spectroscopic analyses of over 100 SDSS/SEGUE stars, and claims that the SSPP is able to determine  $T_{\text{eff}}$ ,  $\log$

$g$ , and  $[\text{Fe}/\text{H}]$  to precisions of 141 K, 0.23 dex, and 0.23 dex, respectively, after combining small systematic offsets quadratically for stars with  $4500 \text{ K} \leq T_{\text{eff}} \leq 7500 \text{ K}$ .

Paper II shows how to select likely member stars of globular (M15, M13, and M2) and open (NGC 2420 and M67) clusters, utilizing the SDSS photometry and spectroscopy, and uses them to derive an overall metallicity of each cluster to validate the parameter-estimating ability of the SSPP, in particular,  $[\text{Fe}/\text{H}]$ . The results of a comparison of the calculated overall metallicities of the clusters to literature values suggest that the metallicities derived by the SSPP have the typical external uncertainties of 0.13 dex, for a wide range of colors ( $-0.3 \leq g-r \leq 1.3$ ), down to a spectroscopic signal-to-noise of  $S/N = 10/1$ . Paper III describes how the high-resolution spectra of the SDSS/SEGUE stars were analyzed and provides a more thorough comparison with the SSPP parameters. The quoted errors of the parameters derived by the SSPP in that paper are  $\sigma(T_{\text{eff}}) = 130 \text{ K}$ ,  $\sigma(\log g) = 0.21 \text{ dex}$ , and  $\sigma([\text{Fe}/\text{H}]) = 0.11 \text{ dex}$ , which slightly differ from those obtained by Paper I, although they share a common set of high-resolution calibration observations. This is due to the fact that Paper III derived the external uncertainties of the SSPP by only taking into account the stars observed with the Hobby Eberly Telescope (HET; Ramsey et al. 1998), while Paper I considered all available high-resolution spectra, including the sample referred to as OTHERS in Paper III, which exhibits somewhat larger scatter in its parameters when compared with those determined by the SSPP.

After adding five more GCs (M71, M3, M53, M92, and NGC 5053) and three more open clusters (M35, NGC 2158, and NGC 6791), another round of validation of the metallicity determined by the SSPP is performed in Paper IV, which makes use of the same approach as in Paper II to select the likely member stars of each cluster and to compute the overall metallicity. This paper confirms that the typical scatter of the SSPP-derived  $[\text{Fe}/\text{H}]$  is in the order of  $\sim 0.1 \text{ dex}$ , as in Paper II. An appendix in Paper IV provides additional information on the techniques used for the parameter averaging, and on changes made to the SSPP since Paper I. In particular, the re-calibration of the metallicity estimated by the NGS1 and NGS2 approaches results in improved metallicity determinations for the metal-poor ( $[\text{Fe}/\text{H}] < -2.0$ ) and metal-rich ( $[\text{Fe}/\text{H}] \sim 0.0$ ) extremes (see Table 4 and the appendix of Paper IV).

Although the resolution of the SDSS/SEGUE spectra is too low to determine abundances for individual  $\alpha$ -elements, we have sought to estimate averaged  $[\alpha/\text{Fe}]$  ratios by inspection of a specific wavelength range over which  $\alpha$ -element-sensitive features are found. The large dataset from SDSS/SEGUE with available  $[\alpha/\text{Fe}]$  estimates is well suited for finding rare objects with low or high  $\alpha$ -element abundances, as well as for tracing the general trends associated with different stellar populations.

In this paper, we describe a method for the determination of  $[\alpha/\text{Fe}]$  from low-resolution SDSS/SEGUE spectra, and our efforts to validate this technique, so that meaningful results can

be obtained not only for stars in the thin- and thick-disk components of the Galaxy, but also for stars that are members of the halo populations. Our validation relies on comparisons with degraded spectra for stars with known  $[\alpha/\text{Fe}]$  ratios taken from the ELODIE spectral library (Moultaka et al. 2004), a sub-sample of 91 of the roughly 350 SDSS/SEGUE stars for which we have obtained high-resolution follow-up spectra to date, and likely members of GCs and OCs with known  $[\alpha/\text{Fe}]$  ratios for which the SEGUE spectra have been obtained. Section 2 describes our adopted technique for estimation of  $[\alpha/\text{Fe}]$  for the SEGUE stellar spectra, while the validation exercise is described in Section 3. Tests of the reliability of our method, in particular its sensitivity to S/N and degeneracies between surface gravity, metallicity, and the derived  $[\alpha/\text{Fe}]$  ratios, are explored in Section 4. Section 5 presents a short summary and conclusions.

## 2. Methodology

### 2.1. Grid of Synthetic Spectra

In order to obtain a fast, robust estimate of  $[\alpha/\text{Fe}]$  ratios for the SEGUE spectra, we make use of a pre-existing grid of synthetic spectra. This eliminates the need for generating synthetic spectra on the fly, while simultaneously attempting to determine the primary atmospheric parameters.

We have made use of Kurucz’s NEWODF atmospheric models (Castelli & Kurucz 2003), with no enhancement of  $\alpha$ -element abundances. These models employ solar relative abundances from Grevesse & Sauval (1998), under the assumption of plane-parallel line-blanketed model structures in one-dimensional local thermodynamical equilibrium (LTE), and include  $\text{H}_2\text{O}$  opacity, an improved set of TiO lines, and no convective overshoot (Castelli et al. 1997). The ready made models can be downloaded from Kurucz’s Website<sup>12</sup>. We adopted these models to generate a finer grid (steps of 0.2 dex for  $\log g$  and 0.2 dex for  $[\text{Fe}/\text{H}]$ ) by linear interpolation between the wider model grids (which have original steps of 0.5 dex).

Note that although there exist atmospheric models with  $\alpha$ -element enhancements, we have chosen not to use them, in order to avoid abrupt changes in the model atmospheres introduced when interpolating to obtain a finer grid in  $[\alpha/\text{Fe}]$ . Employing a homogeneous set of model atmospheres also ensures smooth changes in  $\chi^2$  space as the parameters are estimated. As a check on the impact of this choice, we compared some synthetic spectra generated with  $\alpha$ -enhanced models to those without  $\alpha$ -enhanced models, and found that the mean difference in the flux between them is much less than 1%, with a standard deviation smaller than 1%. Thus, the choice has minimal effect on the determination of  $[\alpha/\text{Fe}]$ .

---

<sup>12</sup><http://kurucz.harvard.edu/grids.html>

We created synthetic spectra from this finer grid using the `turbospectrum` synthesis code (Alvarez & Plez 1998), which uses the treatment of line broadening described by Barklem & O’Mara (1998), along with the solar abundances of Asplund et al. (2005). The sources of atomic lines used by `turbospectrum` come largely from the VALD database (Kupka et al. 1999). Line lists for the molecular species CH, CN, OH, TiO, and CaH are provided by Plez (see Plez & Cohen 2005, and B. Plez, private communication), while the lines of NH, MgH, and the C<sub>2</sub> molecules are adopted from the Kurucz line lists<sup>13</sup>.

When synthesizing the spectra we increase, by the same amount, the abundances for the  $\alpha$ -elements (O, Mg, Si, Ca, and Ti). A micro-turbulence of  $2 \text{ km s}^{-1}$  is adopted for all spectra, as at resolving power  $R = 2000$  the spectral features do not change measurably with differently assumed values of the micro-turbulence (because the micro-turbulence mostly influences the strong spectral lines). The generated synthetic spectra have wavelength steps of  $0.1 \text{ \AA}$ . This wavelength interval was chosen after considering the total computing time required for carrying out the syntheses, and the fact that we found little or no difference in the spectral line shapes for degraded synthetic spectra formed by starting with steps smaller than  $0.1 \text{ \AA}$ . For example, we found that the maximum difference in flux between a spectrum with  $0.1 \text{ \AA}$  and  $0.005 \text{ \AA}$  steps, after smoothing to  $R = 2000$ , is usually less than 2%, and only increases to about 5% for a cool metal-rich giant (e.g.,  $T_{\text{eff}} = 4000 \text{ K}$ ,  $\log g = 1.0$ ,  $[\text{Fe}/\text{H}] = +0.4$ ), located at the very edge of the parameter space of our grid.

Each synthetic spectrum covers the wavelength range  $4500 - 5500 \text{ \AA}$ . This wavelength range was chosen because it contains a large set of metallic lines, but avoids the CH *G* band ( $4300 \text{ \AA}$ ), which is often a strong feature in metal-poor stars, and the Ca II K ( $\sim 3933 \text{ \AA}$ ) and H ( $\sim 3968 \text{ \AA}$ ) lines, which become problematic for cool metal-rich stars due to saturation of these lines. Most importantly, this region includes prominent Mg I and Ti I and Ti II lines (see Figure 1), which are very sensitive features for estimation of the  $\alpha$ -abundance.

The final grid covers  $4000 \text{ K} \leq T_{\text{eff}} \leq 8000 \text{ K}$  in steps of  $250 \text{ K}$ ,  $0.0 \leq \log g \leq 5.0$  in steps of  $0.2 \text{ dex}$ , and  $-4.0 \leq [\text{Fe}/\text{H}] \leq +0.4$  in steps of  $0.2 \text{ dex}$ . The range in  $[\alpha/\text{Fe}]$  introduced for the spectral synthesis covers  $-0.1 \leq [\alpha/\text{Fe}] \leq +0.6$ , in steps of  $0.1 \text{ dex}$ , at each node of  $T_{\text{eff}}$ ,  $\log g$ , and  $[\text{Fe}/\text{H}]$ . After creation of the full set of synthetic spectra, they are degraded to SEGUE resolution ( $R = 2000$ ) and re-sampled to  $1 \text{ \AA}$  wide linear pixels (during SSPP processing, the SEGUE spectra are also linearly re-binned to  $1 \text{ \AA}$  per pixel).

We do not attempt to determine the abundance of individual  $\alpha$ -elements; rather, we attempt to quantify their overall behavior. Hence, our notation  $[\alpha/\text{Fe}]$  refers to an average of the abundance ratios for individual  $\alpha$ -elements, weighted by their line strengths in synthesized spectra. As the dominant features in the spectral range we have selected are Mg and Ti lines, these elements are

---

<sup>13</sup><http://kurucz.harvard.edu/LINELISTS/LINESMOL/>

certainly the primary contributors to our determination of  $[\alpha/\text{Fe}]$ , although Si and Ca may have some influence, as seen in Figure 1.

It is clear that, if a star has very different abundances for the four individual  $\alpha$ -elements we consider (for the generation of synthetic spectra, our assumption is that the abundances of the four elements vary in lockstep), our measured  $[\alpha/\text{Fe}]$  may not correctly represent the overall content of the  $\alpha$ -elements, especially in cases of abnormally low (or high) Mg or Ti abundances, since our technique relies heavily on the Mg and Ti lines.

Since O presents no strong detectable features in this wavelength range (at this resolution) we exclude the O abundance when combining the  $\alpha$ -element abundances from the literature to compute the overall  $\alpha$ -element abundance, expressed as  $[\alpha/\text{Fe}]$ , as we validate our measured  $[\alpha/\text{Fe}]$  with the stars in other external sources such as the ELODIE spectral library.

Owing to the different line strengths of each  $\alpha$ -element in the spectral window used to estimate  $[\alpha/\text{Fe}]$ , we place different weights on each element, and then compute the weighted mean of  $[\alpha/\text{Fe}]$  and its standard deviation for the literature values in order to validate our method of determining  $[\alpha/\text{Fe}]$ :

$$\langle x \rangle = \frac{\sum_{i=1}^n w_i x_i}{\sum_{i=1}^n w_i}, \quad (1)$$

$$\sigma^2 = \frac{\sum_{i=1}^n w_i (x_i - \langle x \rangle)^2}{\sum_{i=1}^n w_i}, \quad (2)$$

where  $x_i$  is replaced by  $[\text{Mg}/\text{Fe}]$ ,  $[\text{Ti}/\text{Fe}]$ ,  $[\text{Ca}/\text{Fe}]$ , or  $[\text{Si}/\text{Fe}]$ , with weighting factors  $w_i = 5, 3, 1$ , or  $1$ , respectively;  $\langle x \rangle$  is  $[\alpha/\text{Fe}]$ . This weighting system was determined after examination of line strengths (equivalent widths, EWs) of individual  $\alpha$ -elements shown in Figure 1. From the grid of synthetic spectra, we calculated the EW of each line listed in Figure 1, summed up all EWs for all lines for each element, and determined an averaged ratio of the summed EWs of each element to the total EWs of all four elements. Through these computations we obtained ratios of 0.50 for Mg, 0.33 for Ti, 0.08 for Ca, and 0.09 for Si (rounded to 0.5 for Mg, 0.3 for Ti, 0.1 for Ca, and 0.1 for Si). For elements without reported abundances in the literature for a given star, zero weight is assigned ( $w_i = 0$ ). When less than four elements are reported, the individual weights change accordingly, so that the sum of the weights always adds to unity.

## 2.2. Preprocessing Target and Synthetic Spectra

The initial steps for the determination of  $[\alpha/\text{Fe}]$  for the SEGUE spectra are to transform the wavelength scale to an air-based (rather than the original SDSS vacuum-based) scale, and to shift the spectrum to the rest frame using the radial velocity delivered by the SSPP. Following these steps, the spectrum is linearly re-binned to 1 Å pixels over the wavelength range 4500 – 5500 Å.

The spectrum under consideration is then normalized by dividing its reported flux by its pseudo-continuum shape. The pseudo-continuum over the 4500 – 5500 Å range is obtained by carrying out an iterative procedure that rejects points lying more than  $1\sigma$  below and  $4\sigma$  above the fitted function, obtained from a 9th-order polynomial. Although we have a “perfect” continuum available for a given synthetic spectrum, the synthetic spectra used to match with the observed spectra are normalized in exactly the same fashion as for the observed spectra, over the same wavelength range, and with the same pixel size. Application of the same continuum routine ensures the same magnitude of line-strength suppression in both spectra.

## 2.3. Determination of $[\alpha/\text{Fe}]$

Following the above steps, we then search the grid of synthetic spectra for the best-fitting model parameters. In this approach, we seek to minimize the distance between the normalized target flux,  $T$ , and the normalized synthetic flux,  $S$ , as functions of  $T_{\text{eff}}$ ,  $\log g$ ,  $[\text{Fe}/\text{H}]$ , and  $[\alpha/\text{Fe}]$ , using a reduced  $\chi^2$  criterion:

$$\chi^2 = \frac{1}{m-n} \sum_{i=1}^m (T_i - S_i)^2 / \sigma_i^2, \quad (3)$$

where  $\sigma_i$  is the error in flux in the  $i$ th pixel,  $m$  is the number of data points, and  $n$  is the degrees of freedom. The SDSS/SEGUE spectra provide the error in the flux associated with each pixel.

The parameter search over the reduced  $\chi^2$  space is performed by the IDL function minimization routine AMOEBA, which uses a downhill simplex method (Nelder & Mead 1965). In this search process, we fix  $T_{\text{eff}}$  to the value determined (previously) by the SSPP, and change  $\log g$ ,  $[\text{Fe}/\text{H}]$ , and  $[\alpha/\text{Fe}]$  simultaneously to minimize  $\chi^2$ , rather than vary all four parameters at once. Since temperature has (by far) the largest effect on the appearance of a stellar spectrum over the wavelength range we consider, holding it constant permits the more subtle variations associated with the other parameters to be explored. Note that even though we adopt for convenience the notation “SSPP” parameters in the figures and tables in this paper, we make use of the parameters ( $\log g$ ,  $[\text{Fe}/\text{H}]$ , and  $[\alpha/\text{Fe}]$ ) determined by this method to compare and validate, except  $T_{\text{eff}}$ ,

which comes directly from the SSPP. It should be also kept in mind that as this technique shares the same grid of synthetic spectra as in NGS2, one of the parameter searching techniques in the SSPP, we apply the same correction function (Equation (A2) in Paper IV) which was derived by re-calibrating the metallicity of the method to  $[\text{Fe}/\text{H}]$  determined by this method.

Figure 2 provides examples of the results of our spectral fitting method. The left-hand panel shows an observed spectrum (black line) for a mildly  $\alpha$ -enhanced metal-poor dwarf, while the right-hand panel corresponds to a slightly cooler, low  $\alpha$ -abundance, metal-rich dwarf. The red dashed line is the synthetic spectrum generated with the parameters listed in each panel, while  $\log g$ ,  $[\text{Fe}/\text{H}]$ , and  $[\alpha/\text{Fe}]$  are determined by the method described above ( $T_{\text{eff}}$  is delivered by the SSPP). From inspection, one can see that an excellent match between the synthetic and observed spectra is achieved for these two stars. The distribution of residuals shown at the bottom of each panel indicates that the largest deviations for individual features are no more than a few percent in the case of the metal-poor dwarf, and no more than five percent for the metal-rich dwarf.

Errors associated with the determination of  $[\alpha/\text{Fe}]$  are estimated as follows. We begin with the reported uncertainty associated with each pixel, as delivered from the SDSS pipelines, and construct 10 different realizations of the noise flux, assuming that the uncertainty is a  $1\sigma$  error of a Gaussian distribution. Then, after adding (or subtracting) these noise fluxes to the observed flux, we follow the method described above to determine  $[\alpha/\text{Fe}]$ . Following this procedure, we have 10 different estimates of  $[\alpha/\text{Fe}]$ ; the random error associated with the measured  $[\alpha/\text{Fe}]$  is taken to be the standard deviation of these different estimates. A more detailed discussion of uncertainties in the  $[\alpha/\text{Fe}]$  determination is addressed below.

### 3. Validation of the Method

Once a technique to determine a physical quantity ( $[\alpha/\text{Fe}]$  in this case) is constructed, it must be calibrated and validated with external measurements. Rather than comparing the overall properties of a sample of stars, it is preferable to compare star-by-star, ideally against different sources, in order to quantify possible systematic offsets (and optionally remove them), as well as to determine the likely random errors associated with the estimate. For these purposes we employ the ELODIE spectral library (Moultaka et al. 2004), as well as a set of SDSS/SEGUE stars observed at moderately high dispersion ( $R \sim 15,000$ ) with the High Resolution Spectrograph (HRS; Tull 1998) on the HET (Ramsey et al. 1998) and at medium resolution ( $R = 6000$ ) with the Echelle Spectrograph and Imager (ESI; Sheinis et al. 2002) on the Keck telescope. For convenience, in this paper we refer to the spectra of SDSS/SEGUE stars observed with the HET as “HET” spectra (data, or stars); those observed on the Keck are referred to as “ESI” spectra (data, or stars). In addition to the above samples,  $[\alpha/\text{Fe}]$  ratios for likely member stars of the Galactic GCs (M15,

M13, and M71) and OCs (NGC 2420, M67, and NGC 6791) having SDSS/SEGUE spectra are compared with published average values of  $[\alpha/\text{Fe}]$  for each cluster.

### 3.1. Comparison with the ELODIE Spectral Library

Spectra in the publicly available ELODIE library (we used version ELODIE.3.1; Moulta et al. 2004), were obtained with the ELODIE spectrograph at the Observatoire de Haute-Provence 1.93 m telescope, and cover the spectral region 4000 – 6800 Å. As the higher resolution spectra (with resolving power  $R = 42,000$ ) are already normalized to a pseudo-continuum, we employed the spectra with  $R = 10,000$ . Most of the spectra have quite high S/N ratios ( $> 100 - 200/\text{Å}$ ), and are accompanied by estimated stellar parameters (not including  $[\alpha/\text{Fe}]$ ) from the literature. Each spectrum (and parameter estimate) has a quality flag assigned to it, ranging from 0 to 4, with 4 being best. In our comparison exercise, we only select stars with  $4000 \text{ K} \leq T_{\text{eff}} \leq 8,000 \text{ K}$  with a quality flag  $\geq 1$  for the spectra and all of the parameters. The temperature range corresponds to that covered by the grid of the synthetic spectra employed in our approach.

Although the spectra come with  $T_{\text{eff}}$ ,  $\log g$ , and  $[\text{Fe}/\text{H}]$  estimates from other studies and from the ELODIE library’s own measurement, the catalog does not supply  $[\alpha/\text{Fe}]$  measurements. The “known”  $\alpha$ -element abundances for the selected spectra are obtained from a literature search, using the VizieR<sup>14</sup> database. The elemental abundances for these stars are based on high-resolution analyses from various studies. Even though there may exist systematics in the compiled  $\alpha$ -element abundances between individual studies, we do not attempt to adjust for any potential offsets from study to study. As mentioned by Venn et al. (2004, and references therein), the study-to-study and model-to-model variations in these abundances could potentially be as large as 0.1 – 0.2 dex.

From Equations (1) and (2) we obtain a weighted average (and standard deviation) of the available  $\alpha$ -element measurements among Mg, Ti, Ca, and Si for a given star, and represent them as  $[\alpha/\text{Fe}]$  and its error in our subsequent analysis. Because some of the reported abundances among the four elements are not accompanied by errors in the source papers, to report the uncertainties in a consistent manner we conservatively estimate the uncertainty in the reported  $[\alpha/\text{Fe}]$  from the standard deviation of the different reported values of the four individual abundances. Recall that we do not consider the O abundance, because the wavelength region chosen for our analysis does not include any strong O lines.

We attempt to only use stars for which the abundances of at least three  $\alpha$ -elements are available; the Mg abundance must exist among the three, and the abundance of the  $\alpha$ -elements should

---

<sup>14</sup><http://webviz.u-strasbg.fr/viz-bin/VizieR>

also lie within the range of our grid,  $-0.1 \leq [\alpha/\text{Fe}] \leq +0.6$ . However, as we find that most of metal-poor stars ( $[\text{Fe}/\text{H}] < -1.5$ ) in the ELODIE spectra have only a reported Mg abundance, and they are valuable sources of validation for our technique, we adopt  $[\text{Mg}/\text{Fe}]$  as an estimate of  $[\alpha/\text{Fe}]$  in order to include them in our comparisons ( $[\alpha/\text{Fe}]$  uncertainties are not reported for those stars in Table 1).

Following these procedures, we have compiled a list of 293 unique stars with good quality spectra (generally this corresponds to  $S/N > 100/\text{\AA}$ ), with atmospheric parameters in the range of our synthetic grid, and with available information from which the determination of  $[\alpha/\text{Fe}]$  can be made. There are multiple spectral observations made for some stars in the ELODIE spectra; we analyze the individual spectra in our comparisons as they are good sources of consistency checks on the derived parameters. Because of the inclusion of multiple spectra for some stars, the total number of spectra considered in the comparison (425) is much larger than the number of unique stars. Figure 3 shows the parameter space that the ELODIE sample spans. Clearly, we see there are not many cool metal-poor or metal-rich giants. The lack of metal-poor giants is partially filled by the high-resolution sample discussed below.

The spectra of the stars from the sample meeting our desired criteria are processed in the same way as the synthetic spectra used for spectral matching, after degrading them to  $R = 2000$  using a Gaussian kernel and re-sampling to  $1 \text{ \AA}$  per pixel in the spectral range  $4500 - 5500 \text{ \AA}$ ;  $[\alpha/\text{Fe}]$  for the selected stars is then estimated. It should be noted that, due to the limited spectral range of the ELODIE spectra compared with that of the SEGUE spectra, it is not possible to process these spectra through the SSPP to obtain the stellar parameters, in particular  $T_{\text{eff}}$ , which is necessary to estimate  $[\alpha/\text{Fe}]$  with our method. Therefore, we adopt  $T_{\text{eff}}$  from the literature value reported in the ELODIE spectra, and hold it fixed during the  $\chi^2$  minimization scheme.

Concerning error estimates for  $[\alpha/\text{Fe}]$ , as the ELODIE spectra do not provide explicit errors in the flux for each pixel of a given spectrum, we conservatively assume a 1% error (which is a reasonable assumption as  $S/N$  is  $100/1 - 200/1$  for all spectra), and attempt to determine measured errors in  $[\alpha/\text{Fe}]$  following the procedure outlined in Section 2.3. Table 1 lists all the stars with the parameters adopted in our comparison, including our measured parameters.

Figure 4 illustrates the results of our comparisons with the selected ELODIE stars. “ELODIE” indicates the value of  $[\alpha/\text{Fe}]$  obtained from the literature, while “SSPP” denotes our determination. The left-hand diagram of the figure is a Gaussian fit to the residuals between our values and those from the literature; an overall offset of  $-0.010$  dex is found, along with a scatter of  $0.062$  dex. The right-hand panel plots our measurements against the literature values, and a one-to-one correspondence line. There is no obvious deviation in our determination along the perfect correlation line. For the sake of clarity, error bars for each star in Figure 4 are suppressed, and a typical total error bar in our measured  $[\alpha/\text{Fe}]$  and the literature values is denoted in the lower right corner of the

right-hand panel of the figure.

Figure 5 displays residuals in  $[\alpha/\text{Fe}]$  between our derived values and the ELODIE-derived values as a function of  $T_{\text{eff}}$ ,  $\log g$ , and  $[\text{Fe}/\text{H}]$  from upper to lower panels. Although it appears that there is a small downward trend at low  $T_{\text{eff}}$  ( $< 4800$  K) and our estimated  $[\alpha/\text{Fe}]$  tends to be higher at  $[\text{Fe}/\text{H}] < -2.3$ , the deviations seen at such low  $T_{\text{eff}}$  and  $[\text{Fe}/\text{H}]$  are mostly consistent with zero within the measured errors, suggesting that there is no obvious correlation along with each parameter.

As the uncertainty in our measured  $[\alpha/\text{Fe}]$  consists of both systematic and random errors, and the abundances that we employ from the literature (based on the high-resolution analysis) also have uncertainties, we quantify the total error in our measurement of  $[\alpha/\text{Fe}]$  by the following procedure. Let  $\sigma_{\text{g}}$  be the rms scatter from a Gaussian fit to the residuals between our measurements and the literature values of  $[\alpha/\text{Fe}]$ , and  $\sigma_{\text{HR}}$  be the error from the literature estimate calculated from Equation (2). Then the systematic error ( $\sigma_{\text{sys}}$ ) in our measured  $[\alpha/\text{Fe}]$  is derived by

$$\sigma_{\text{sys}}^2 = \sigma_{\text{g}}^2 - \sigma_{\text{HR}}^2 - \sigma_{\text{SSPP}}^2, \quad (4)$$

where  $\sigma_{\text{SSPP}}$  is the random error, simply taken to be the internal uncertainty of our technique, estimated by following the procedure outlined in Section 2.3. In this equation,  $\sigma_{\text{HR}}$  and  $\sigma_{\text{SSPP}}$  are an individual value for each target, whereas a value of  $\sigma_{\text{g}}$  from the full sample is used. That is,  $\sigma_{\text{g}}$  is fixed for all spectra, while  $\sigma_{\text{HR}}$  and  $\sigma_{\text{SSPP}}$  change for each star. If  $\sigma_{\text{HR}}$  is not available for a star, then we plug into the equation an average of  $\sigma_{\text{HR}}$  from the sample. Using this relation, we compute an overall systematic error in our measured  $[\alpha/\text{Fe}]$  by means of taking average of the sample, and define it as  $\langle \sigma_{\text{sys}} \rangle$ . This  $\langle \sigma_{\text{sys}} \rangle$  is applied to individual spectra to yield the total error in our measurement of  $[\alpha/\text{Fe}]$  for each object by the following equation:

$$\sigma_{\text{tot}}^2 = \langle \sigma_{\text{sys}} \rangle^2 + \sigma_{\text{SSPP}}^2. \quad (5)$$

In the equations above, the largest contribution to the total error ( $\sigma_{\text{tot}}$ ) comes from the scatter between our measured values and the literature ones ( $\sigma_{\text{g}}$ ). However, if the noise in a given spectrum dominates, the random error of ( $\sigma_{\text{SSPP}}$ ) contributes more to the total error; this is discussed further in Section 4.1.

The error bars in Figure 5 are obtained from the quadratic addition of our measured total error to the literature error. Note that, as mentioned earlier, there are some stars without properly measured errors. For those stars, we adopt an average  $[\alpha/\text{Fe}]$  uncertainty based on all stars with available error estimates. We also notice from Figure 4 that the mean offset ( $-0.010$  dex) is negligible, so we do not take it into account in our total error calculations. We obtain 0.054 dex as the

typical total error in our  $[\alpha/\text{Fe}]$  estimates for the ELODIE spectra (obtained from a simple average of the total errors for all stars considered in the figure). The systematic error ( $\langle \sigma_{\text{sys}} \rangle$ ) for the ELODIE spectra is 0.044 dex. The rms scatter between this method and the literature is 0.092 dex for  $\log g$  and 0.122 dex for  $[\text{Fe}/\text{H}]$ , suggesting that the technique is robust for the estimation of other parameters as well as for simultaneously determining  $[\alpha/\text{Fe}]$ .

All error bars in  $[\alpha/\text{Fe}]_{\text{SSPP}}$  in the figures and the quoted total errors of our estimated  $[\alpha/\text{Fe}]$  in the tables in this paper are calculated from Equations (4) and (5) above.

### 3.2. Comparison with SDSS/SEGUE High-resolution Spectra

The optimal test of our ability to predict  $[\alpha/\text{Fe}]$  ratios from the SEGUE spectra comes from a comparison with that obtained from analysis of higher-resolution spectra observed for the same stars. Fortunately, a large number of suitable spectra were obtained during the course of our efforts to calibrate atmospheric parameters for the SSPP. We discuss this comparison below. Detailed information on these high-resolution spectra and their analysis can be found in Papers III and IV, which validate (calibrate) the stellar parameters determined by the SSPP by comparison with the high-dispersion spectra.

The general procedure for estimating  $[\alpha/\text{Fe}]$  for the HET spectra is very similar to the analysis described in Paper III. The only differences are that a slightly smaller wavelength window is used, and the inclusion of O, Mg, Si, Ca and Ti elements, all with the same level of enhancement. The determination of  $[\alpha/\text{Fe}]$  is performed by minimizing  $\chi^2$  between the HET spectra and the model fluxes, as in Paper III, but holding  $T_{\text{eff}}$  constant at the value determined in Paper III, and fitting  $\log g$ ,  $[\text{Fe}/\text{H}]$ , and  $[\alpha/\text{Fe}]$  simultaneously. In this process, the internal error in each parameter is derived from the square root of the diagonal elements of the covariance matrix. The estimated  $[\text{Fe}/\text{H}]$  and  $\log g$  from this minimization are consistent with those found in Paper III (the rms scatter between them is 0.05 dex for  $[\text{Fe}/\text{H}]$  and 0.16 dex for  $\log g$ , respectively).

We set the zero point for the  $[\alpha/\text{Fe}]$  values by forcing  $[\alpha/\text{Fe}] = 0$  at  $[\text{Fe}/\text{H}] = 0$ , which requires applying an offset of 0.13 dex over the entire metallicity range to the  $[\alpha/\text{Fe}]$  values determined directly from the analysis. This zero-point offset is independent of any other parameter and likely results from the usual approximations, in particular the use of a one-dimensional atmospheric structure in Local Thermodynamic Equilibrium (LTE). Allende Prieto (2006) addressed the offsets in  $[\alpha/\text{Fe}]$  at  $[\text{Fe}/\text{H}] = 0$  in several surveys, and whether they might signal that the Sun is somewhat chemically peculiar (see also Gustafsson 1998). His conclusion was that when solar analogs were examined (that is, when the effective temperature, surface gravity, and overall metal content of the stars were restricted to a narrow interval around the solar parameters) the offsets went away. This

is the primary motivation for removing the 0.13 dex offset in our case.

From this analysis, we have obtained a total of 73 HET stars with well-measured parameters, including  $[\alpha/\text{Fe}]$ , in the range of our grid ( $-0.1 \leq [\alpha/\text{Fe}] \leq +0.6$ ).

For the ESI spectra, Lai et al. (2009) describe the methods for determining the stellar parameters, including the  $\alpha$ -element abundances; we refer interested readers to that paper. The abundances of Mg, Ti, and Ca are available for the ESI stars, so we place zero weight on Si and the same weighting factors (5, 3, and 1) on the others as before. Following Equations (1) and (2), we calculate  $[\alpha/\text{Fe}]$  and its standard deviation for each star and collect a total of 18 stars with available parameters within the boundaries of our grid of synthetic spectra. The ESI data are mostly metal-poor giants, and provide a useful sample to validate our technique for very metal-poor stars with low surface gravity, filling the hole in the parameter space explored by the ELODIE sample. Taken together with the HET spectra, we have a total of 91 stars with which to compare. Table 2 lists these stars, along with the parameters and their associated errors from the high-resolution analysis and from our measurements.

Figure 6 displays the range of the parameters for the high-resolution sample. We note that the ESI data (gray squares) nicely cover the gap in the cool metal-poor giant region, missing in Figure 3, but there remains a lack of cool metal-rich giants. We attempt to address the defect in this regime by comparison with a metal-rich open cluster, NGC 6791, in the following section.

Figure 7 illustrates the results of the comparison of our derived  $[\alpha/\text{Fe}]$  with the high-resolution determinations. Black dots represent the HET stars, while the gray squares indicate the ESI stars. The notation “HR” denotes the high-resolution determinations; “SSPP” refers to our results from the low-resolution SEGUE spectra. A Gaussian fit to the residuals, shown in the left-hand panel, suggests a mean offset of 0.003 dex and a standard deviation of 0.069 dex, respectively, rather similar to those found from the comparison with the ELODIE spectra. Using Equations (4) and (5), we compute the total error bar on the measured  $[\alpha/\text{Fe}]$  and place it in the figure.

Examination of Figure 8 reveals no strong correlations between our measured residuals of  $[\alpha/\text{Fe}]$  with  $T_{\text{eff}}$ ,  $\log g$ , and  $[\text{Fe}/\text{H}]$ , within our derived errors, although there may be a slight tendency toward lower  $[\alpha/\text{Fe}]$  determinations at the lowest temperatures ( $T_{\text{eff}} < 4750$  K), gravities ( $\log g < 1.8$ ), and metallicities ( $[\text{Fe}/\text{H}] < -2.5$ ), mainly for ESI stars. These behaviors provide information on the limitations of our technique over the parameter space. Thus, based on present information, our method may not work for the coolest metal-poor giant stars ( $T_{\text{eff}} < 4800$  K,  $\log g < 2.0$ , and  $[\text{Fe}/\text{H}] < -2.5$ ). These tendencies are, of course, also a natural consequence of using low-resolution spectra to determine the  $\alpha$ -abundances, as there exist few sensitive spectral features of the  $\alpha$ -elements for such low gravity, metal-poor stars. Clearly, additional comparison stars with low temperature, gravity, and metallicity would be useful to set the effective range of

the parameter space for the measured  $[\alpha/\text{Fe}]$ . Nevertheless, as we can obviously separate out the low- $\alpha$  stars from the high- $\alpha$  ones, we regard the parameter coverage of the high-resolution sample as the valid range of our method.

For clarity in the plots in both Figures 7 and 8, we only show the vertical error bars; the typical error bar from the high-resolution analysis for each parameter is displayed in the lower-right corner of each panel. From this comparison, we derive 0.062 dex as a typical total error in the estimated  $[\alpha/\text{Fe}]$  for the HET and ESI stars, which is commensurate with that estimated from our analysis of the ELODIE spectra. The computed  $\langle \sigma_{\text{sys}} \rangle$  for this sample (0.048 dex) is in good agreement with that of the ELODIE dataset (0.044 dex). The deviation scatter between this method and the high-resolution analysis is 0.274 dex for  $\log g$  and 0.175 dex for  $[\text{Fe}/\text{H}]$ , which are somewhat larger than those from the ELODIE comparison. This is partly due to the fact that we adopt  $T_{\text{eff}}$  from the literature to run our technique and that the ELODIE spectra have much higher S/N.

Considering the results from both the ELODIE and high-resolution spectra comparisons, we conclude that, in addition to reproducing the scatter of  $\log g$  and  $[\text{Fe}/\text{H}]$  from the SSPP (less than 0.3 dex and 0.2 dex, respectively), we are able to estimate  $[\alpha/\text{Fe}]$  with a precision on the order of 0.06 dex from SDSS/SEGUE spectra with  $\text{S/N} > 50/1$  (note that the SEGUE spectra for all of the HET and ESI stars had high S/N, driven by the selection of brighter stars for high-resolution observation).

### 3.3. Comparison with Likely Member Stars of Globular and Open Clusters

Stars in Galactic GCs and OCs provide a good testbed for validation of the stellar atmospheric parameters, as in most clusters it is expected that the member stars were born simultaneously out of well-mixed, uniform-abundance gas at the same location in the Galaxy. Hence, member stars should exhibit very similar elemental-abundance patterns. Note that even though there is evidence for internal variations in the abundances of light elements in GCs (notably C and N; Cohen et al. 2005), since the spectral region we utilize does not contain any significant C or N lines, our measured parameters are not affected by this variation. This statement also holds true for Na and Al, which exhibit star-to-star variations in the GCs (e.g., Carretta et al. 2009a, 2009b; references therein), as the wavelength window for measuring  $[\alpha/\text{Fe}]$  does not include any strong lines of these two elements. One concern in the use the GCs as external calibrators is that there is some evidence that there may exist a variation in  $[\text{Mg}/\text{Fe}]$  associated with Na and Al anomalies, especially for M13 (Johnson et al. 2005). However, as we are attempting to measure the overall content of the  $\alpha$ -elements, not only the Mg abundance, the internal dispersion of  $[\alpha/\text{Fe}]$  due to possible variations of Mg abundances in the cluster will be mitigated, so we include the GC member stars to compare with our derived  $[\alpha/\text{Fe}]$ .

During the course of the SDSS and SEGUE surveys, we have secured photometric and spectroscopic data for stars in the vicinity of several globular and OCs. A subset of these clusters, M15, M13, M71, NGC 2420, M67, and NGC 6791, have published high-resolution spectroscopic determinations of  $\alpha$ -abundances that we use to compare with our estimates from the low-resolution SEGUE spectra.

Following the procedures in Paper II and Paper IV, which describe how we select likely member stars in the GCs and OCs and use them to validate the stellar parameters delivered by the SSPP, we first select likely member stars for each cluster. We obtain totals of 59 (M15), 217 (M13), 17 (M71), 125 (NGC 2420), 52 (M67), and 88 (NGC 6791) respectively, of likely members with  $[\alpha/\text{Fe}]$  determination based on spectra having an average of  $S/N > 20/1$  per pixel. We then calculate the weighted average  $\langle[\alpha/\text{Fe}]\rangle$  and its scatter for each cluster, following Equations (1) and (2). In this case,  $x_i$  is the  $[\alpha/\text{Fe}]$  estimate and  $w_i = 1/\sigma_i^2$ ,  $\sigma_i$  being the error in  $[\alpha/\text{Fe}]$  of the  $i$ th star. The error in the calculated mean ( $\langle[\alpha/\text{Fe}]\rangle$ ) is computed from:

$$\sigma_{\langle x \rangle}^2 = \frac{1}{\sum_{i=1}^n 1/\sigma_i^2}. \quad (6)$$

To obtain the literature value of  $[\alpha/\text{Fe}]$  for each cluster, we have searched for high-resolution studies in the literature on each cluster for any available abundances of Mg, Ti, Ca, and Si, and compute the weighted mean of  $[\alpha/\text{Fe}]$  from Equation (1). As the error in each elemental abundance is provided in all cases, the error in the weighted mean of  $[\alpha/\text{Fe}]$  is calculated by the following equation:

$$\sigma^2 = \frac{\sum_{i=1}^n (w_i x_i)^2}{(\sum_{i=1}^n w_i)^2}, \quad (7)$$

where  $x_i$  is substituted by the error in the Mg, Ti, Ca, Si abundances. The same weighting factors ( $w_i$ ) are applied as for the ELODIE and ESI spectra discussed above. Table 3 summarizes the derived means and errors in the mean of  $[\alpha/\text{Fe}]$  from the literature values and from our likely member stars for each cluster, along with the literature and our derived estimates of  $[\text{Fe}/\text{H}]$ . Sources for the literature values are listed in the table notes.

Figure 9 shows, from top to bottom, the distribution of the estimated  $[\alpha/\text{Fe}]$  for the selected member stars of M15, M13, M71, NGC 2420, M67, and NGC 6791 as a function of  $(g-r)_0$  (left-hand panels),  $\log g$  (middle panels), and the average signal-to-noise ratio per pixel,  $\langle S/N \rangle$  (right-hand panels). The dashed line is the weighted mean from the literature, while the solid line is our weighted average of  $[\alpha/\text{Fe}]$  of the likely member stars. The weighted averages ( $\langle[\alpha/\text{Fe}]\rangle$ ) of  $[\alpha/\text{Fe}]$  from the literature are listed at the top of each middle panel; our weighted means ( $\mu$ ) and

scatter ( $\sigma$ ) for each cluster are listed at the top of each right-hand panel. The mean metallicity of each cluster adopted from the literature is also displayed at the top of each left-hand panel. The typical error bar, shown in the lower-left corner of the left-hand panels, is obtained by quadratically adding the random error of each member star and the systematic error (0.054 dex) derived from the HET and ESI data.

Inspection of Figure 9 indicates that our derived means agree very well with those from the high-resolution analyses up to super solar metallicity ( $\sim +0.5$ ), except perhaps for the GC M15. As there are not many high-resolution studies performed on this cluster, only two studies (Sneden et al. 1997 and Sneden et al. 2000) were first considered to derive the literature abundance of the  $\alpha$ -elements. However, we compute the mean  $[\alpha/\text{Fe}]$  from Sneden et al. (1997), which reports the abundances for the four  $\alpha$ -elements, because the other study does not report Mg abundance, which has the largest contribution on computing  $[\alpha/\text{Fe}]$ . The apparently large discrepancy in M15 shown in Figure 9 is due to the high  $[\text{Si}/\text{Fe}]$  (+0.60) and  $[\text{Ti}/\text{Fe}]$  (+0.46) ratios measured by Sneden et al. (1997). The abundances of these two elements also exhibit large star-to-star scatter in their study, which they attribute to observational error. It will be interesting to see how the mean values change when  $\alpha$ -abundances from future high-resolution observations become available. It is worth noting that our measured mean  $[\alpha/\text{Fe}]$  (+0.24) is much closer to that (+0.33) of Kirby et al. (2008a), who derived their estimate from 44 stars in M15 using a very similar method to ours, albeit applied to higher resolution spectra ( $R = 6000$ ) in a redder spectral region (6300–9100 Å). Their average value of  $[\alpha/\text{Fe}]$  is shown as the dash-dotted line in Figure 9.

It should also be noted that the overall metallicity of NGC 2420 derived by Pancino et al. (2010) in Table 3 is relatively higher (by about 0.3 to 0.4 dex) than other studies (e.g., Friel & Janes 1993; Friel et al. 2002; Anthony-Twarog et al. 2006), which are based on medium-resolution spectra or intermediate-band photometry. Their value is also larger by  $\sim 0.2$  dex than that of another high-resolution study by H. Jacobson et al. (2010, in preparation), ( $-0.22 \pm 0.07$ ), who used nine ( $R = 21,000$ ) spectra of giants to calculate the average metallicity. Their overall metallicity is in fact much closer to ours ( $-0.25$ ) in Table 3. This cluster clearly requires more high-resolution studies to confirm its mean metallicity. As Pancino et al. (2010) provide the mean  $[\alpha/\text{Fe}]$  of the cluster with the overall  $[\text{Fe}/\text{H}]$ , we adopt it in the table.

It is noteworthy that Figure 9 shows that even some cool metal-rich giants in NGC 6791 exhibit good agreement (within  $2\sigma$ , considering the rms scatter), as these stars could be considered supplementary objects to the high-resolution sample (which lacks cool metal-rich stars). Also notice that although our grid of synthetic spectra reaches up to  $[\text{Fe}/\text{H}] = +0.4$ , Table 3 lists +0.428 as the overall metallicity of the cluster. This arises from applying the correction function for metallicity to the  $[\text{Fe}/\text{H}]$  determined by this method, as explained in Section 2.3.

Further inspection of Figure 9 reveals that the uncertainty in the measured  $[\alpha/\text{Fe}]$  increases

for more metal-deficient stars, as expected due to the overall weakness of the lines involved in its estimation. However, no obvious covariance in the reported  $[\alpha/\text{Fe}]$  with respect to  $(g-r)_0$ ,  $\log g$ , and  $\langle S/N \rangle$  is noticed, although the random scatter around the mean increases at lower  $S/N$  for high-gravity blue stars, especially in metal-poor cases (M13 and M15). This emphasizes the difficulty of obtaining reliable  $[\alpha/\text{Fe}]$  for faint, metal-poor main-sequence turnoff and dwarf stars.

## 4. Reliability of $[\alpha/\text{Fe}]$ Estimation from SDSS/SEGUE Spectra

### 4.1. Effects of Declining Signal-to-noise Ratios

While the two data sets (the ELODIE spectra and the SDSS/SEGUE stars with parameters estimated from the high-resolution analysis) used for the validation of our technique have very high  $S/N$  ( $> 100/1$  for the ELODIE spectra, much higher than that when smoothed to the SDSS resolution, and  $> 50/1$  for the SDSS/SEGUE stars with high-resolution spectra), the low-resolution SDSS/SEGUE spectra cover a wide range of  $S/N$ . Thus, it is desirable to check the impact that lower  $S/N$  for a given spectrum has on estimation of  $[\alpha/\text{Fe}]$ . Following the prescriptions described in Paper I, we perform noise-injection experiments on the ELODIE spectra<sup>15</sup> and the SDSS/SEGUE spectra of the stars with high-resolution observations. Among the SDSS/SEGUE stars with high- and medium-resolution spectroscopy available, only those with stellar parameters determined from analysis of the HET data had noise-added spectra available, so we just consider this subset of the ELODIE and the SDSS/SEGUE spectra in this experiment.

Table 4 summarizes the results. The mean offset ( $\Delta$ ) and the standard deviation ( $\sigma$ ) for each parameter are derived from a Gaussian fit to the residuals between our results and the external sources listed in the table. The effective temperature with the subscript “SSPP” is the adopted value from the SSPP (which was held fixed for the determination of  $[\alpha/\text{Fe}]$ ). The listed  $\sigma_{\text{tot}}$  is the average total error in  $[\alpha/\text{Fe}]$ , calculated following Equations (4) and (5). The label “Full” in the column listing  $S/N$  indicates that the parameters are derived from the spectra prior to noise injection.

---

<sup>15</sup>The noise-added spectra, and more detailed information on noise models can be found at <ftp://hebe.as.utexas.edu/pub/callende/sdssim/>.

#### 4.1.1. HET Comparison

From inspection of Table 4, the effective temperature from the SSPP that we fix to predict  $[\alpha/\text{Fe}]$  exhibits a systematic offset of about 130 K, with a scatter of 180 K, from high to low S/N; we do not correct for this offset when estimating  $[\alpha/\text{Fe}]$ . This offset has a small dependence on  $T_{\text{eff}}$ , but not on  $\log g$ , nor  $[\text{Fe}/\text{H}]$ . If we add the ESI data, the offset becomes about 140 K, as seen in Table 5, and depends only very slightly on temperature below  $T_{\text{eff}} < 5000$  K, as the ESI spectra mostly contain cool stars. Nonetheless, this temperature offset does not grossly impact on our derived  $\log g$ ,  $[\text{Fe}/\text{H}]$ , and  $[\alpha/\text{Fe}]$ , as can be deduced from Table 5. More discussion on this point is given below.

One can also notice an offset of about 0.1 dex in  $\log g$ , relative to the SSPP values, decreasing as the S/N decreases, albeit with larger scatter. For  $[\text{Fe}/\text{H}]$ , the offset generally increases, with larger scatter, as the quality of the spectrum decreases. We see the same trend for  $[\alpha/\text{Fe}]$  in Table 5. Although there indeed exist small systematic offsets in  $T_{\text{eff}}$ ,  $\log g$ , and  $[\text{Fe}/\text{H}]$  (of slightly different size) at different values of S/N, these offsets do not appear to impact estimates of  $[\alpha/\text{Fe}]$ ; only small offsets ( $< 0.01$  dex), with a relatively small scatter ( $< 0.1$  dex) are found for our  $[\alpha/\text{Fe}]$  determinations down to  $\text{S/N} = 20$ .

It is also clear that our technique reproduces  $\log g$  and  $[\text{Fe}/\text{H}]$  reasonably well, as the rms scatter between the high-resolution analysis and our results is  $< 0.3$  dex for  $\log g$  and  $< 0.2$  dex for  $[\text{Fe}/\text{H}]$  down to about  $\text{S/N} = 20$ .

#### 4.1.2. ELODIE Comparison

For the ELODIE stars, Table 4 exhibits much smaller offsets and scatters for all three parameters,  $\log g$ ,  $[\text{Fe}/\text{H}]$ , and  $[\alpha/\text{Fe}]$ . The small offsets and scatters are the natural consequence of adopting  $T_{\text{eff}}$  from the literature, and holding it fixed while estimating  $[\alpha/\text{Fe}]$ , rather than using the internally determined  $T_{\text{eff}}$ .

Interpreting the results of the noise-injection tests from both the HET and ELODIE samples, we can infer that at high S/N the dominant error in the total uncertainty is the systematic error,  $\langle \sigma_{\text{sys}} \rangle$  in Equation (5), while at low S/N the random internal error,  $\sigma_{\text{SSPP}}$  in Equation (5), is the dominant error, as the total error starts smaller and becomes larger with declining S/N, as can be seen in Table 4.

We also conclude from the noise-injection experiments that we are able to estimate  $[\alpha/\text{Fe}]$  with a precision of  $< 0.1$  dex down to  $\text{S/N} = 20/1$ , while reproducing  $\log g$  and  $[\text{Fe}/\text{H}]$  estimates within about 0.3 and 0.2 dex, respectively, at the same S/N. We emphasize that, although the results of the

ELODIE comparisons appear better behaved, the quoted scatters from the comparisons with the high-resolution analysis are more realistic, since we adopt the  $T_{\text{eff}}$  derived by the SSPP to determine  $[\alpha/\text{Fe}]$ , whereas the  $T_{\text{eff}}$  provided in the literature was used for the ELODIE stars.

Some additional caution should be exercised in the interpretation of these results, since relatively metal-rich stars (with  $[\text{Fe}/\text{H}] > -1.4$ ) dominate in both samples, as can be appreciated by inspection of Figures 5 and 8. We might expect that the error in the determination of  $[\alpha/\text{Fe}]$  varies with the metallicity of a star such that the uncertainty of  $[\alpha/\text{Fe}]$  will be larger in the metal-poor stars than for the metal-rich stars, as the metallic line strengths become weaker. Additional noise in the spectrum of a metal-poor star will drive the uncertainty to even higher values. Owing to the scarcity of metal-poor stars in our comparison samples, we are not able to carry out a thorough test on the dependency of the uncertainty in the measured  $[\alpha/\text{Fe}]$  with metallicity. Nevertheless, by only taking into account stars with  $[\text{Fe}/\text{H}] < -1.4$  at  $\text{S/N} = 25$  and calculating the total error in the derived  $[\alpha/\text{Fe}]$ , we obtain  $\sigma_{\text{tot}} = 0.112$  dex for the HET stars and 0.108 dex for the ELODIE stars. Thus, for the present, we suggest that spectra of at least  $\text{S/N} = 25/1$  are required to achieve total errors in the estimated  $[\alpha/\text{Fe}]$  on the order of 0.1 dex for low-metallicity stars ( $[\text{Fe}/\text{H}] < -1.4$ ). The limiting lower metallicity over which our determinations of  $[\alpha/\text{Fe}]$  can be made will surely vary with effective temperature (we expect sufficient line strengths of the  $\alpha$ -element features to allow determinations for cooler stars down to  $[\text{Fe}/\text{H}] \sim -3.0$ , but perhaps not for warmer stars below  $[\text{Fe}/\text{H}] = -2.5$ ). Additional exploration will be necessary to be certain.

## 4.2. Degeneracy Effects Among Parameters

Within the spectral window (4500 – 5500 Å) chosen to estimate  $[\alpha/\text{Fe}]$ , the Mg *Ib* and MgH lines are the dominant contributors to our estimates of  $[\alpha/\text{Fe}]$ . These spectral features are also sensitive to the surface gravity and overall metallicity of a given star, as illustrated in Figure 1. The  $\alpha$ -elements are also good indicators of metallicity. Thus, one has to be concerned about possible degeneracies among the derived stellar parameters and  $[\alpha/\text{Fe}]$ . In other words, does the application of our approach make it possible for an  $\alpha$ -enhanced giant to be interpreted as a dwarf with a low  $[\alpha/\text{Fe}]$  ratio? Or can a metal-rich low- $\alpha$  star be identified as a metal-deficient star due to weakness of the  $\alpha$ -element spectral features through application of our techniques?

We confront this issue by considering the HET and ESI data, which contain both dwarfs and giants covering a range of metallicities. We examine this sample, looking for stars that are misclassified as a result of covariance between surface gravity and the effect of  $\alpha$ -element variations on the strength of, e.g., the Mg lines. Recall that we have already considered in Figure 8 the distribution of  $[\alpha/\text{Fe}]$  residuals between the high-resolution analysis and our low-resolution analysis as a function of  $T_{\text{eff}}$ ,  $\log g$ , and  $[\text{Fe}/\text{H}]$ , for different ranges of each parameter, and found that there

was no significant correlations with each parameter.

Figure 10 shows variations in  $[\alpha/\text{Fe}]$  as functions of the residuals between our analysis and the high-resolution analysis of  $T_{\text{eff}}$ ,  $\log g$ , and  $[\text{Fe}/\text{H}]$ , from the upper to the lower panels. The dashed lines are  $\pm 2\sigma_{\text{tot}}$  ( $\sigma_{\text{tot}} = 0.062$  dex) derived in Section 3.2. For clarity, error bars of the residuals of each parameter are not plotted for each star; instead, an average error is drawn in the lower-right corner of each panel. Scrutinizing the top panel of the figure reveals that, although there are a handful of stars that deviate by more than 300 K, differences in the  $[\alpha/\text{Fe}]$  estimates for these stars is mostly well within  $\pm 3\sigma_{\text{tot}}$  with the allowed error bars. Specifically, among the stars within  $\pm 300$  K, 57% are inside  $\pm 1\sigma_{\text{tot}}$ , 89% for  $\pm 2\sigma_{\text{tot}}$ , and 97% for  $\pm 3\sigma_{\text{tot}}$  without taking into account the error bars. If we remove the systematic shift in  $T_{\text{eff}}$  (about 140 K from Table 5), almost all stars fall into the range  $\pm 300$  K.

The middle panel of Figure 10 indicates that the surface gravity determined by our method mostly agrees with the high-resolution analysis within  $\pm 0.5$  dex. Even though there are a few stars with apparently large deviations ( $> 0.5$  dex) in surface gravity with respect to the high-resolution analysis, no star in this sample would have its classification changed from a dwarf to a giant, or vice versa. Furthermore, the great majority of stars have  $[\alpha/\text{Fe}]$  differences that fall well inside  $\pm 3\sigma_{\text{tot}}$ ; we obtain that 61%, 93%, and 99% of the stars within  $\pm 0.5$  dex reside inside 1, 2, and  $3\sigma_{\text{tot}}$  levels, respectively. This suggests that even if the gravity determination is off by over 0.5 dex, the estimated  $[\alpha/\text{Fe}]$  is not significantly impacted by more than  $3\sigma_{\text{tot}}$ . Note that even for the very low gravity stars ( $\log g \sim 1.5$ ) seen in Figure 8, we consistently obtain a good agreement with the high-resolution results.

The lower panel of Figure 10 shows that the metallicity determined by our technique is mostly consistent with the high-resolution analysis within  $\pm 0.3$  dex. In this range, 69% of the stars are inside  $\pm 1\sigma_{\text{tot}}$ , 89% for  $\pm 2\sigma_{\text{tot}}$ , and 97% for  $\pm 3\sigma_{\text{tot}}$ . Moreover, since almost all stars have  $[\alpha/\text{Fe}]$  differences that fall well inside  $\pm 3\sigma_{\text{tot}}$ , it is clear that variations in the line strengths of the  $\alpha$ -elements do not result in large perturbations in the derived metallicity estimates. This is likely the result of the application of multiple methods in the SSPP for the determination of  $[\text{Fe}/\text{H}]$ .

The confirmations from both cases above imply that we are indeed measuring an  $[\alpha/\text{Fe}]$  ratio, rather than obtaining spurious estimates due to shifts of the other parameters, such as  $\log g$  and  $[\text{Fe}/\text{H}]$ , that compensate for differences in the  $\alpha$ -element line strengths. It is very unlikely that our analysis would allow a high- $[\alpha/\text{Fe}]$  giant to masquerade as a low- $[\alpha/\text{Fe}]$  dwarf, or vice versa. Similarly, we would not expect a metal-rich low- $\alpha$  star to be identified as a metal-deficient star, due to weakness of the  $\alpha$ -element spectral features, through the application of our techniques.

However, as discussed in Section 3.2, there does appear to exist a weak tendency (when excluding the stars with large error bars) that if our estimates of  $T_{\text{eff}}$ ,  $\log g$ , or  $[\text{Fe}/\text{H}]$  are higher

than the high-resolution values, then the determined  $[\alpha/\text{Fe}]$  is slightly lower than that obtained from the high-resolution analysis. The stars which display that trend are mostly cool metal-poor giants, and due to statistically small sample of such stars, it is hard to tell how much the behavior significantly affects our results. A supplementary set of high-resolution spectra of cool metal-poor stars may be useful to clarify this.

Similar checks have been performed for the ELODIE spectra; Figure 11 displays the results. In this figure we do not compare against  $T_{\text{eff}}$ , because, as mentioned previously, we adopt  $T_{\text{eff}}$  from the literature (and hold it fixed during the  $[\alpha/\text{Fe}]$  determination). The dashed lines are  $\pm 2\sigma_{\text{tot}}$  ( $\sigma_{\text{tot}} = 0.055$  dex), as calculated in Section 3.2. As can be appreciated from inspection of the upper panel, no stars exhibit gravity differences with respect to the literature values larger than 0.5 dex; only a few stars deviate by more than 0.3 dex in the metallicity differences from the literature values, as seen in the lower panel. These two panels clearly imply that there is a very tight distribution in the metallicity and the gravity differences with respect to the literature values, with only a few stars exhibiting  $[\alpha/\text{Fe}]$  differences larger than  $3\sigma_{\text{tot}}$ .

We conclude from these experiments that our determination of  $[\alpha/\text{Fe}]$  is robust over a wide range of surface gravity ( $1.5 \leq \log g \leq 5.0$ ) and metallicity ( $-3.0 \leq [\text{Fe}/\text{H}] \leq +0.3$ ), and that it is not unduly influenced by possible degeneracies between absorption lines with sensitivity to surface gravity and metallicity as well as to  $[\alpha/\text{Fe}]$ . This is confirmed by Figure 9; down to  $\log g = 2$  there is no manifest trend of  $[\alpha/\text{Fe}]$  with the gravity estimate, only the random scatter around the mean of  $[\alpha/\text{Fe}]$  varies. The results for NGC 6791 provide evidence that the metallicity range of our technique may extend to  $\sim +0.5$ .

### 4.3. Effects of Errors in $T_{\text{eff}}$ on Determination of $[\alpha/\text{Fe}]$

During the process of carrying out the minimum  $\chi^2$  search, we have fixed  $T_{\text{eff}}$  at the value determined by the SSPP, and only allow the other three parameters,  $\log g$ ,  $[\text{Fe}/\text{H}]$ , and  $[\alpha/\text{Fe}]$ , to be solved for simultaneously. However, since the effective temperature estimate delivered by the SSPP itself carries uncertainty, we need to check on how this error in  $T_{\text{eff}}$  propagates into uncertainties in the determination of  $[\alpha/\text{Fe}]$ . We perform this test (using the HET and ESI spectra) by varying the adopted  $T_{\text{eff}}$  by  $-300$ ,  $-200$ ,  $-100$ ,  $+100$ ,  $+200$ , and  $+300$  K from the value suggested by the SSPP. Table 5 summarizes the results of this experiment, and gives the derived variations in the estimated  $\log g$  and  $[\text{Fe}/\text{H}]$ , and  $[\alpha/\text{Fe}]$ . All the listed mean offsets and standard deviations in the table are derived from Gaussian fits to the residual distributions.

There exists (as we have previously pointed out) a systematic offset of about 140 K in  $T_{\text{eff}}$  between the SSPP and the high-resolution analysis, even when no perturbation is applied to the fixed

$T_{\text{eff}}$  when evaluating  $[\alpha/\text{Fe}]$ , as discussed in Section 4.1.1. Hence, this test is also useful to estimate how the temperature offset influences our derived quantities of  $\log g$ ,  $[\text{Fe}/\text{H}]$ , and  $[\alpha/\text{Fe}]$ . According to Table 5, even if we adjust the offset by 100 K or 200 K, we do not notice much change of the rms scatter in each parameter. At maximum, about 0.025 dex in  $[\text{Fe}/\text{H}]$  for the adjustment of  $-200$  K is notable. This confirms that the temperature offset has only a very minor impact on our measured parameters.

Table 5 also allows us to infer that for all three derived parameters the mean offsets associated with different input offsets in  $T_{\text{eff}}$  are rather small, and all cases are less than the derived rms variation in the determinations of these parameters. Accordingly, it appears that within  $\pm 300$  K (which is a bit larger than the typical error of 250 K of the SSPP-determined  $T_{\text{eff}}$ ), the  $[\alpha/\text{Fe}]$  estimate is perturbed by less than  $\pm 0.1$  dex, which is smaller than  $2\sigma_{\text{tot}}$ . This implies that our approach to deriving  $[\alpha/\text{Fe}]$  is robust against small deviations of the estimated temperature.

## 5. Summary and Conclusions

We have presented a method for estimating  $[\alpha/\text{Fe}]$  from the low-resolution ( $R = 2000$ ) SDSS/SEGUE stellar spectra, based on spectral matching against a grid of synthetic spectra. Star-by-star comparisons with spectra from a degraded ELODIE spectral library (with  $[\alpha/\text{Fe}]$  calculated from literature values of individual  $\alpha$ -element abundances) and with the SEGUE spectra of stars with high-resolution determinations of  $[\alpha/\text{Fe}]$ , indicate that this approach is capable of estimating  $[\alpha/\text{Fe}]$  with a precision of  $< 0.07$  dex for spectra with  $S/N > 50/1$  over the parameter space  $T_{\text{eff}} = [4500, 7000]$  K,  $\log g = [1.5, 5.0]$ ,  $[\text{Fe}/\text{H}] = [-3.0, +0.3]$ , and  $[\alpha/\text{Fe}] = [-0.1, +0.6]$ . According to our noise-injection experiments, errors in the determination of  $[\alpha/\text{Fe}]$  increase to  $> 0.1$  dex for  $S/N < 15/1$ . Thus, for application of this approach, we recommend that spectra with a minimum  $S/N = 20/1$  be used. From close examination of a small sample of metal-poor stars ( $[\text{Fe}/\text{H}] < -1.4$ ), we have found that it is desirable to have spectra with  $S/N > 25/1$  for such stars to achieve an uncertainty in the measured  $[\alpha/\text{Fe}]$  comparable to 0.1 dex. Using our methods, we obtained  $\sigma_{\text{tot}} = 0.112$  dex from the HET and ESI stars, and 0.108 dex from the ELODIE sample at this  $S/N$  for these metal-poor stars. The question of whether this  $S/N$  limit could be lowered will require a larger number of comparison stars at low metallicity to be considered, an effort that is presently underway.

A validation with likely members of the Galactic GCs M15, M13, and M71 and the OCs NGC 2420, M67, and NGC 6791 confirms that the weighted average  $[\alpha/\text{Fe}]$  for member stars obtained by our measurements is in good agreement with the weighted mean of the literature values, within the reported scatter. The one possible exception is M15, which has a published value for the Mg abundance, with large star-to-star scatters for  $[\text{Si}/\text{Fe}]$  and  $[\text{Ti}/\text{Fe}]$ , based on high-resolution spectroscopy. Our estimate of  $[\alpha/\text{Fe}]$  for this cluster is, however, close to that of Kirby

et al. (2008a), who employed a similar technique as ours for somewhat higher resolution spectra of member stars in M15. The comparison with NGC 6791 implies that the valid range of the metallicity for our method may extend to  $\sim +0.5$ .

We have looked for, and failed to find, any significant covariance between surface gravity and our derived estimates of  $[\alpha/\text{Fe}]$ , which depend on the same spectral features for much of their sensitivity to these parameters. We have also found relatively small variations in  $\log g$  ( $< 0.3$  dex) and  $[\text{Fe}/\text{H}]$  ( $< 0.2$  dex) with  $[\alpha/\text{Fe}]$  (itself mostly exhibiting peak-to-peak scatter of less than  $3\sigma_{\text{tot}}$ ) between our measurements and high-resolution analyses.

We have also checked on possible errors in our determination of  $[\alpha/\text{Fe}]$  due to our choice to fix the input  $T_{\text{eff}}$  to the values delivered by the SSPP (which itself can have errors up to 250 K), and find that for errors less than  $\pm 300$  K, the  $[\alpha/\text{Fe}]$  measurement is perturbed by less than  $\pm 0.1$  dex, which is smaller than  $2\sigma_{\text{tot}}$ .

As this method can be easily applied to other spectra that cover similar wavelength ranges at similar resolving power, it should be a useful new tool for investigation of the star formation and chemical enrichment history of Galactic populations with SDSS/SEGUE, as well as for much larger stellar samples in the future, such as will be obtained from LAMOST.

Funding for the SDSS and SDSS-II has been provided by the Alfred P. Sloan Foundation, the Participating Institutions, the National Science Foundation, the U.S. Department of Energy, the National Aeronautics and Space Administration, the Japanese Monbukagakusho, the Max Planck Society, and the Higher Education Funding Council for England. The SDSS Web site is <http://www.sdss.org/>.

The SDSS is managed by the Astrophysical Research Consortium for the Participating Institutions. The Participating Institutions are the American Museum of Natural History, Astrophysical Institute Potsdam, University of Basel, University of Cambridge, Case Western Reserve University, University of Chicago, Drexel University, Fermilab, the Institute for Advanced Study, the Japan Participation Group, Johns Hopkins University, the Joint Institute for Nuclear Astrophysics, the Kavli Institute for Particle Astrophysics and Cosmology, the Korean Scientist Group, the Chinese Academy of Sciences (LAMOST), Los Alamos National Laboratory, the Max-Planck-Institute for Astronomy (MPIA), the Max-Planck-Institute for Astrophysics (MPA), New Mexico State University, Ohio State University, University of Pittsburgh, University of Portsmouth, Princeton University, the United States Naval Observatory, and the University of Washington.

The Hobby Eberly Telescope (HET) is a joint project of the University of Texas at Austin, the Pennsylvania State University, Stanford University, Ludwig-Maximilians-Universität München, and Georg-August-Universität Göttingen. The HET is named in honor of its principal benefac-

tors, William P. Hobby and Robert E. Eberly. Some of the data presented herein were obtained at the W.M. Keck Observatory, which is operated as a scientific partnership among the California Institute of Technology, the University of California and the National Aeronautics and Space Administration. The Observatory was made possible by the generous financial support of the W.M. Keck Foundation. The authors wish to recognize and acknowledge the very significant cultural role and reverence that the summit of Mauna Kea has always had within the indigenous Hawaiian community. We are most fortunate to have the opportunity to conduct observations from this mountain.

Y.S.L. and T.C.B. acknowledge partial funding of this work from grants PHY 02-16783 and PHY 08-22648: Physics Frontier Center/Joint Institute for Nuclear Astrophysics (JINA), awarded by the U.S. National Science Foundation. H.L.M. acknowledges support from AST-0607518. D.K.L. acknowledges the support of the National Science Foundation through the NSF Astronomy and Astrophysics Postdoctoral Fellowship under award AST-0802292. J.A.J. acknowledges support from NSF grant AST-0607482. We are grateful for the insightful comments of the anonymous referee, which contributed to numerous improvements in our paper.

Table 1. List of Parameters for Selected ELODIE Spectra

ID		ELODIE					SSPP					
	ELODIE	$T_{\text{eff}}$ (K)	$\log g$	[Fe/H]	$[\alpha/\text{Fe}]$	$\sigma_{[\alpha/\text{Fe}]}$ (dex)	$\log g$	$\sigma_{\log g}$ (dex)	[Fe/H]	$\sigma_{[\text{Fe}/\text{H}]}$ (dex)	$[\alpha/\text{Fe}]$	$\sigma_{[\alpha/\text{Fe}]}$ (dex)
HD000245	00001	5433	3.50	-0.76	+0.34	0.02	3.801	0.015	-0.757	0.036	+0.333	0.031
HD000400	00003	6146	4.09	-0.28	+0.11	0.01	4.060	0.022	-0.290	0.045	+0.106	0.029
HD000693	00004	6156	4.13	-0.42	+0.10	0.03	4.156	0.032	-0.443	0.030	+0.079	0.070
HD001835	00006	5777	4.45	+0.17	+0.01	0.03	4.399	0.010	+0.301	0.037	+0.019	0.023
HD003268	00010	6130	4.01	-0.24	+0.12	0.02	3.991	0.018	-0.177	0.029	+0.040	0.049
HD003567	00012	5991	3.96	-1.25	+0.21	0.03	3.930	0.023	-1.434	0.042	+0.177	0.037
HD003628	00013	5701	4.06	-0.19	+0.18	0.07	4.046	0.017	-0.138	0.040	+0.125	0.025
HD004307	00018	5806	4.04	-0.25	+0.03	0.03	4.039	0.021	-0.218	0.032	+0.021	0.027
HD004614	00020	5890	4.40	-0.28	+0.12	0.04	4.372	0.009	-0.193	0.021	+0.063	0.035
HD006582	00028	5313	4.40	-0.83	+0.36	0.03	4.558	0.023	-0.975	0.055	+0.251	0.059
HD006582	00029	5313	4.40	-0.83	+0.36	0.03	4.537	0.007	-0.869	0.057	+0.396	0.016
HD006920	00032	5808	3.47	-0.11	+0.08	0.07	3.485	0.020	-0.220	0.044	+0.094	0.035
HD009562	00034	5821	3.98	+0.15	+0.08	0.07	3.983	0.012	+0.290	0.071	+0.010	0.040
HD009562	00035	5821	3.98	+0.15	+0.08	0.07	4.000	0.036	+0.278	0.041	+0.015	0.049
HD010145	00038	5673	4.40	-0.01	+0.12	0.02	4.482	0.015	-0.155	0.048	+0.079	0.016
HD010307	00039	5862	4.27	+0.00	+0.09	0.05	4.249	0.016	+0.041	0.023	+0.059	0.050
HD010476	00041	5206	4.34	-0.03	+0.07	0.04	4.452	0.015	+0.078	0.068	+0.052	0.043
HD010700	00042	5313	4.32	-0.52	+0.32	0.07	4.475	0.014	-0.676	0.024	+0.352	0.030
HD010780	00043	5369	4.31	+0.05	+0.06	0.06	4.429	0.013	+0.080	0.034	+0.011	0.024
HD013783	00050	5451	4.14	-0.67	+0.39	0.04	4.276	0.015	-0.690	0.047	+0.340	0.031
HD013974	00051	5597	3.92	-0.41	+0.22	0.11	4.111	0.019	-0.461	0.051	+0.102	0.036
HD013974	00052	5597	3.92	-0.41	+0.22	0.11	4.127	0.015	-0.379	0.048	+0.080	0.045

Note. — Note that if only [Mg/Fe] is available from the published studies, no error in  $[\alpha/\text{Fe}]$  is reported, and that there are multiple observations made for some stars. There are 293 unique stars out of 425 spectra. This table is available in its entirety in machine-readable and Virtual Observatory (VO) forms in the online journal. A portion is shown here for guidance regarding its form and content.

Table 2. List of Parameters for HET and ESI Spectra

Plate-MJD-Fiber	SDSS Designation	High-resolution Analysis								SSPP							Ref.	
		$T_{\text{eff}}$ (K)	$\sigma_{T_{\text{eff}}}$ (K)	$\log g$	$\sigma_{\log g}$ (dex)	[Fe/H]	$\sigma_{[\text{Fe}/\text{H}]}$ (dex)	[ $\alpha$ /Fe]	$\sigma_{[\alpha/\text{Fe}]}$ (dex)	$T_{\text{eff}}$ (K)	$\sigma_{T_{\text{eff}}}$ (K)	$\log g$	$\sigma_{\log g}$ (dex)	[Fe/H]	$\sigma_{[\text{Fe}/\text{H}]}$ (dex)	[ $\alpha$ /Fe]		$\sigma_{[\alpha/\text{Fe}]}$ (dex)
0353-51703-605	SDSS J171652.50+603926.9	5672	44	3.372	0.068	-0.350	0.032	+0.082	0.029	6122	46	3.942	0.022	+0.324	0.112	+0.029	0.027	HET
0380-51792-236	SDSS J225801.77+000643.1	6838	90	4.258	0.090	-0.307	0.044	+0.180	0.050	6996	50	4.244	0.031	-0.896	0.161	+0.211	0.035	HET
0396-51816-605	SDSS J010746.51+011402.6	5346	11	4.768	0.088	-0.085	0.018	+0.077	0.046	5416	240	4.902	0.017	+0.060	0.083	+0.029	0.058	HET
0401-51788-407	SDSS J014149.73+010720.2	4876	23	3.151	0.052	-0.452	0.021	+0.351	0.018	4730	100	3.227	0.024	-0.233	0.107	+0.277	0.015	HET
0401-51788-410	SDSS J014215.40+011400.6	5417	40	3.977	0.067	-0.538	0.032	+0.334	0.022	5701	30	4.411	0.014	-0.168	0.044	+0.347	0.020	HET
0409-51871-449	SDSS J024740.30+011144.9	5868	18	4.611	0.123	-0.021	0.027	+0.132	0.044	5705	29	4.584	0.006	+0.165	0.009	+0.022	0.006	HET
0409-51871-562	SDSS J025046.89+010910.8	5527	43	3.836	0.067	-0.873	0.035	+0.355	0.026	5894	19	4.238	0.027	-0.685	0.078	+0.328	0.026	HET
0421-51821-439	SDSS J005826.06+150153.6	5003	26	3.318	0.053	-0.243	0.021	+0.151	0.017	5055	86	3.847	0.020	+0.142	0.104	+0.010	0.046	HET
0434-51885-133	SDSS J074705.19+414452.1	5048	28	3.339	0.056	-0.327	0.023	+0.196	0.018	5049	81	3.765	0.016	-0.178	0.055	+0.112	0.013	HET
0441-51868-497	SDSS J082253.87+471741.9	6042	62	3.994	0.074	-0.653	0.039	+0.153	0.046	6407	38	4.047	0.017	-0.460	0.047	+0.091	0.042	HET
0598-52316-443	SDSS J115520.82+654309.8	5632	49	3.800	0.071	-0.888	0.038	+0.284	0.030	5950	33	4.221	0.016	-0.896	0.060	+0.262	0.028	HET
0604-52079-572	SDSS J134901.58+640924.7	5819	41	4.159	0.060	-0.090	0.028	+0.047	0.022	5946	81	4.567	0.022	+0.088	0.079	+0.118	0.030	HET
0732-52221-345	SDSS J213818.92+123547.8	5192	35	3.728	0.064	-0.699	0.031	+0.391	0.018	5126	44	3.811	0.021	-0.615	0.085	+0.372	0.028	HET
0740-52263-364	SDSS J224610.22+145156.7	5455	26	4.114	0.097	-0.484	0.030	+0.037	0.039	5616	52	4.658	0.017	-0.213	0.040	+0.182	0.036	HET
0744-52251-179	SDSS J231427.16+134821.9	5091	27	3.676	0.051	-0.278	0.021	+0.236	0.016	4976	71	3.837	0.008	-0.026	0.051	+0.079	0.033	HET
0747-52234-136	SDSS J233720.37+140953.8	6444	49	4.470	0.111	-0.141	0.033	+0.059	0.067	6407	45	4.245	0.017	-0.036	0.020	+0.030	0.019	HET
0747-52234-212	SDSS J233611.86+140923.9	5941	51	4.064	0.068	-0.425	0.033	+0.097	0.029	5977	32	4.244	0.030	-0.526	0.049	+0.170	0.029	HET
0781-52373-015	SDSS J124826.99+614358.8	5952	48	3.967	0.066	-0.318	0.031	+0.113	0.029	6133	26	4.229	0.007	-0.225	0.034	+0.072	0.013	HET
0812-52352-578	SDSS J155509.18+495003.3	5638	38	4.332	0.058	-0.365	0.028	+0.141	0.021	5705	34	4.480	0.021	-0.276	0.078	+0.155	0.015	HET
0835-52326-601	SDSS J111901.08+054319.4	5644	15	4.474	0.127	-0.223	0.028	+0.034	0.050	5648	38	4.665	0.019	-0.282	0.043	+0.113	0.028	HET
0888-52339-599	SDSS J074151.21+275319.8	6475	42	4.478	0.159	-0.200	0.036	+0.127	0.138	7120	56	3.954	0.020	-0.635	0.104	+0.132	0.030	HET
0889-52663-204	SDSS J074300.91+285106.6	6348	72	4.247	0.080	-0.496	0.041	+0.100	0.049	6596	32	4.077	0.023	-0.443	0.029	+0.103	0.036	HET

Note. — Note that  $T_{\text{eff}}$  in the SSPP columns is delivered by the SSPP, whereas  $\log g$ , [Fe/H], and [ $\alpha$ /Fe] come from the method described in this paper. The gravity and metallicity of the high-resolution analysis are estimated from the technique addressed in Section 3.2. This table is available in its entirety in machine-readable and Virtual Observatory (VO) forms in the online journal. A portion is shown here for guidance regarding its form and content.

Table 3. Weighted Average [Fe/H] and  $[\alpha/\text{Fe}]$  for Likely Cluster Members

Cluster	Literature			SSPP			
	$\langle [\text{Fe}/\text{H}] \rangle$	$\langle [\alpha/\text{Fe}] \rangle$	$N_{\text{mem}}$	$\langle [\text{Fe}/\text{H}] \rangle$	$\sigma([\text{Fe}/\text{H}])$ (dex)	$\langle [\alpha/\text{Fe}] \rangle$	$\sigma([\alpha/\text{Fe}])$ (dex)
M15	$-2.330 \pm 0.020$	$0.397 \pm 0.149$	59	$-2.170 \pm 0.010$	0.282	$+0.238 \pm 0.006$	0.099
M13	$-1.580 \pm 0.040$	$0.192 \pm 0.017$	217	$-1.567 \pm 0.005$	0.189	$+0.235 \pm 0.003$	0.092
M71	$-0.800 \pm 0.020$	$0.189 \pm 0.189$	17	$-0.755 \pm 0.014$	0.081	$+0.262 \pm 0.010$	0.075
NGC 2420	$-0.050 \pm 0.020$	$0.053 \pm 0.029$	125	$-0.300 \pm 0.006$	0.136	$+0.084 \pm 0.003$	0.044
M67	$+0.030 \pm 0.010$	$0.075 \pm 0.012$	52	$+0.068 \pm 0.007$	0.065	$+0.032 \pm 0.004$	0.027
NGC 6791	$+0.470 \pm 0.070$	$0.093 \pm 0.093$	88	$+0.428 \pm 0.005$	0.084	$+0.027 \pm 0.003$	0.038

Note. — The literature value of  $\langle [\alpha/\text{Fe}] \rangle$  is calculated from the following references—M15: Sneden et al. (1997); M13: Sneden et al. (2004) and Cohen & Meléndez (2005); M71: Boesgaard et al. (2005); NGC 2420: Pancino et al. (2009); M67: Pancino et al. (2010); Yong et al. (2005); Randich et al. (2006); NGC 6791: Carretta et al. (2007). The adopted literature values of [Fe/H] for M15 and M13 come from Carretta et al. (2009c), Boesgaard et al. (2005) for M71, Pancino et al. (2010) for NGC 2420 and M67, and Carretta et al. (2007) for NGC 6791.  $N_{\text{mem}}$  is the total number of the member stars considered in averaging. See the text for methods used to compute the mean and variance from both the literature values and our derived values for each cluster.

Table 4. Variation on Derived Parameters with S/N

S/N	HET									S/N	ELODIE						
	$T_{\text{effSSPP}}$		$\log g$		[Fe/H]		[ $\alpha$ /Fe]				$\log g$		[Fe/H]		[ $\alpha$ /Fe]		
	$\Delta$	$\sigma$	$\Delta$	$\sigma$	$\Delta$	$\sigma$	$\Delta$	$\sigma$	$\sigma_{\text{tot}}$		$\Delta$	$\sigma$	$\Delta$	$\sigma$	$\Delta$	$\sigma$	$\sigma_{\text{tot}}$
(K)	(K)	(dex)	(dex)	(dex)	(dex)	(dex)	(dex)	(dex)	(dex)	(dex)	(dex)	(dex)	(dex)	(dex)	(dex)	(dex)	
10	+155	190	+0.061	0.393	+0.144	0.298	+0.004	0.129	0.122	6.3	+0.019	0.099	+0.758	0.156	-0.004	0.133	0.125
15	+127	182	+0.083	0.325	+0.199	0.193	-0.003	0.106	0.099	12.5	+0.007	0.106	+0.218	0.194	-0.015	0.106	0.098
20	+122	181	+0.088	0.297	+0.185	0.191	-0.003	0.095	0.086	25.0	+0.020	0.100	+0.066	0.126	-0.004	0.076	0.068
25	+132	183	+0.089	0.266	+0.140	0.172	-0.005	0.091	0.083	50.0	+0.023	0.096	+0.004	0.119	-0.001	0.067	0.059
30	+132	182	+0.094	0.257	+0.104	0.172	-0.006	0.088	0.079	Full	+0.035	0.092	+0.019	0.122	-0.010	0.062	0.055
40	+134	175	+0.112	0.251	+0.067	0.176	-0.003	0.088	0.078	...	...	...	...	...	...	...	...
50	+149	174	+0.124	0.247	+0.059	0.177	-0.001	0.085	0.075	...	...	...	...	...	...	...	...
Full	+131	180	+0.124	0.250	+0.019	0.171	+0.005	0.065	0.057	...	...	...	...	...	...	...	...

Note. —  $T_{\text{effSSPP}}$  is the adopted temperature from the SSPP.  $\sigma_{\text{tot}}$  is the total error in the estimated [ $\alpha$ /Fe], computed by Equations (4) and (5).

Table 5. Effects of Errors in  $T_{\text{eff}}$  on Determination of  $[\alpha/\text{Fe}]$

$T_{\text{eff}}$ Error (K)	$T_{\text{eff}}$		$\log g$		[Fe/H]		[ $\alpha/\text{Fe}$ ]		
	$\Delta$ (K)	$\sigma$ (K)	$\Delta$ (dex)	$\sigma$ (dex)	$\Delta$ (dex)	$\sigma$ (dex)	$\Delta$ (dex)	$\sigma$ (dex)	$\sigma_{\text{tot}}$ (dex)
-300	...	...	+0.109	0.266	+0.047	0.210	+0.000	0.087	0.079
-200	...	...	+0.131	0.271	+0.058	0.199	-0.001	0.080	0.072
-100	...	...	+0.124	0.271	+0.047	0.208	-0.007	0.071	0.063
+0	143 <sup>1</sup>	194 <sup>1</sup>	+0.137	0.274	+0.042	0.175	+0.003	0.069	0.062
+100	...	...	+0.144	0.261	+0.044	0.189	+0.002	0.073	0.063
+200	...	...	+0.179	0.269	+0.069	0.190	+0.008	0.094	0.086
+300	...	...	+0.183	0.253	+0.073	0.194	+0.023	0.111	0.099

<sup>1</sup>Gaussian mean and scatter between the SSPP and the high-resolution analysis.

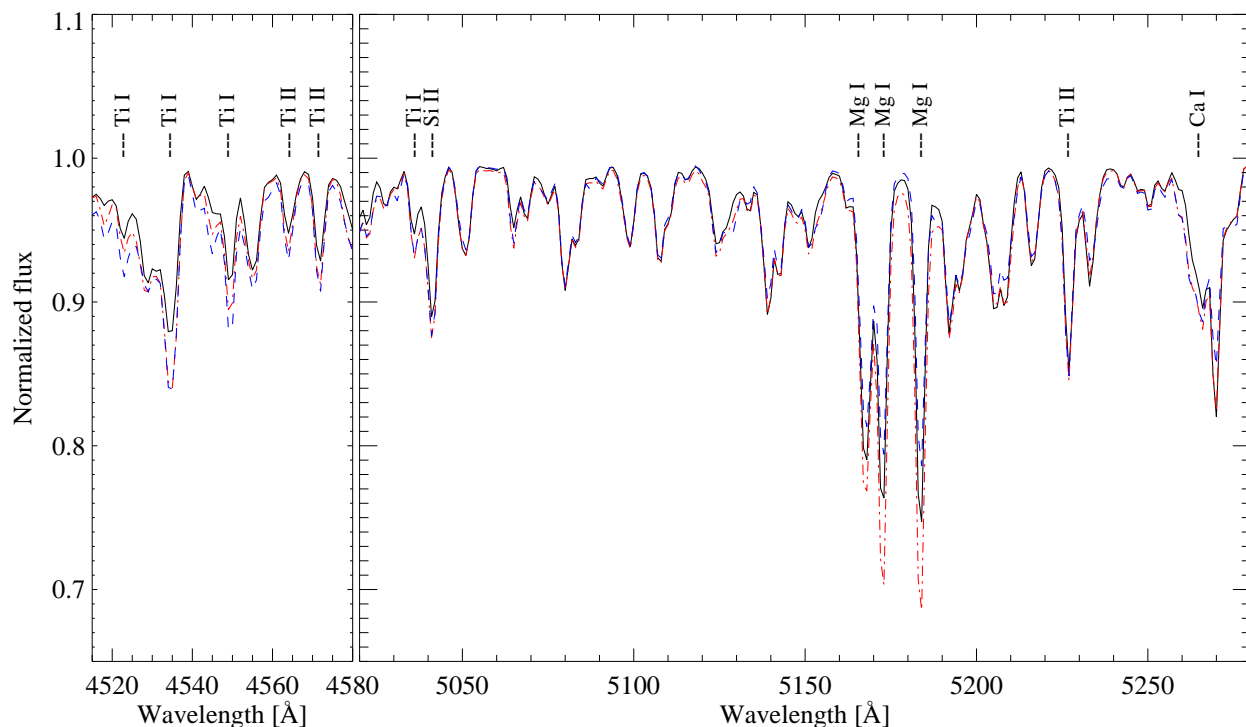


Fig. 1.— Dominant  $\alpha$ -element spectral features in the wavelength window used to determine  $[\alpha/\text{Fe}]$ . The black line shows a synthetic spectrum for a typical dwarf of  $T_{\text{eff}} = 5500$  K,  $\log g = 4.4$ ,  $[\text{Fe}/\text{H}] = -1.4$ , and  $[\alpha/\text{Fe}] = 0.0$ . The red dash-dotted line is the same, except  $[\alpha/\text{Fe}] = +0.4$ . The blue dashed line with  $T_{\text{eff}} = 5500$  K,  $\log g = 3.4$ ,  $[\text{Fe}/\text{H}] = -1.4$ , and  $[\alpha/\text{Fe}] = +0.4$  is also plotted. These spectra are degraded to the SDSS/SEGUE resolution ( $R = 2000$ ). It is clear that Mg and Ti contribute the most to the determination of  $[\alpha/\text{Fe}]$ , and furthermore, it is possible to easily distinguish between the low and high  $\alpha$ -abundance cases. However, it is also noticed that the three Mg I and Ca I line strengths change with gravity.

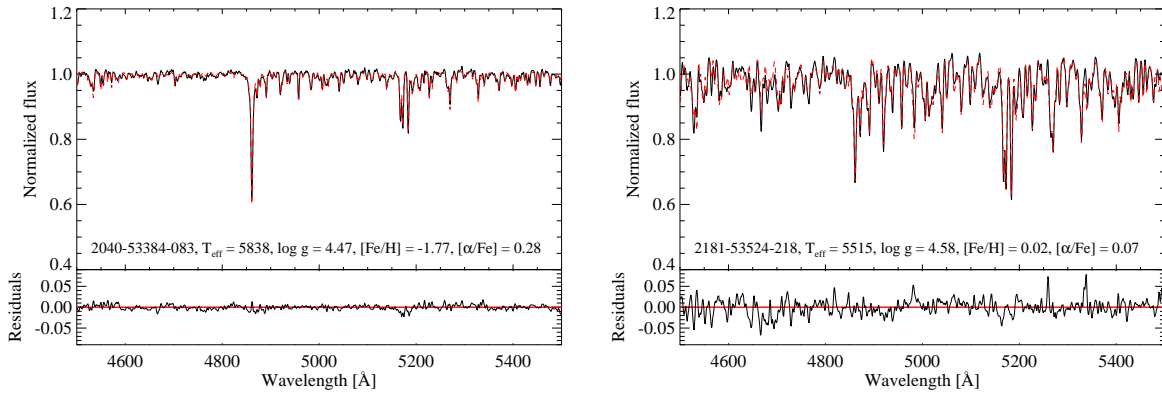


Fig. 2.— Two examples of spectral matching. The left-hand panel shows a metal-poor dwarf, while the right-hand panel shows a metal-rich dwarf. The black line is the observed spectrum, while the red dashed line is the best-matching synthetic spectrum generated with the parameters listed on each plot, as determined by our methodology (with the exception of  $T_{\text{eff}}$ ; see the text). Residuals between the observed and the synthetic spectrum are shown at the bottom of each panel. Note that the largest residuals are no larger than 2% for the metal-poor star and 5% for the metal-rich star.

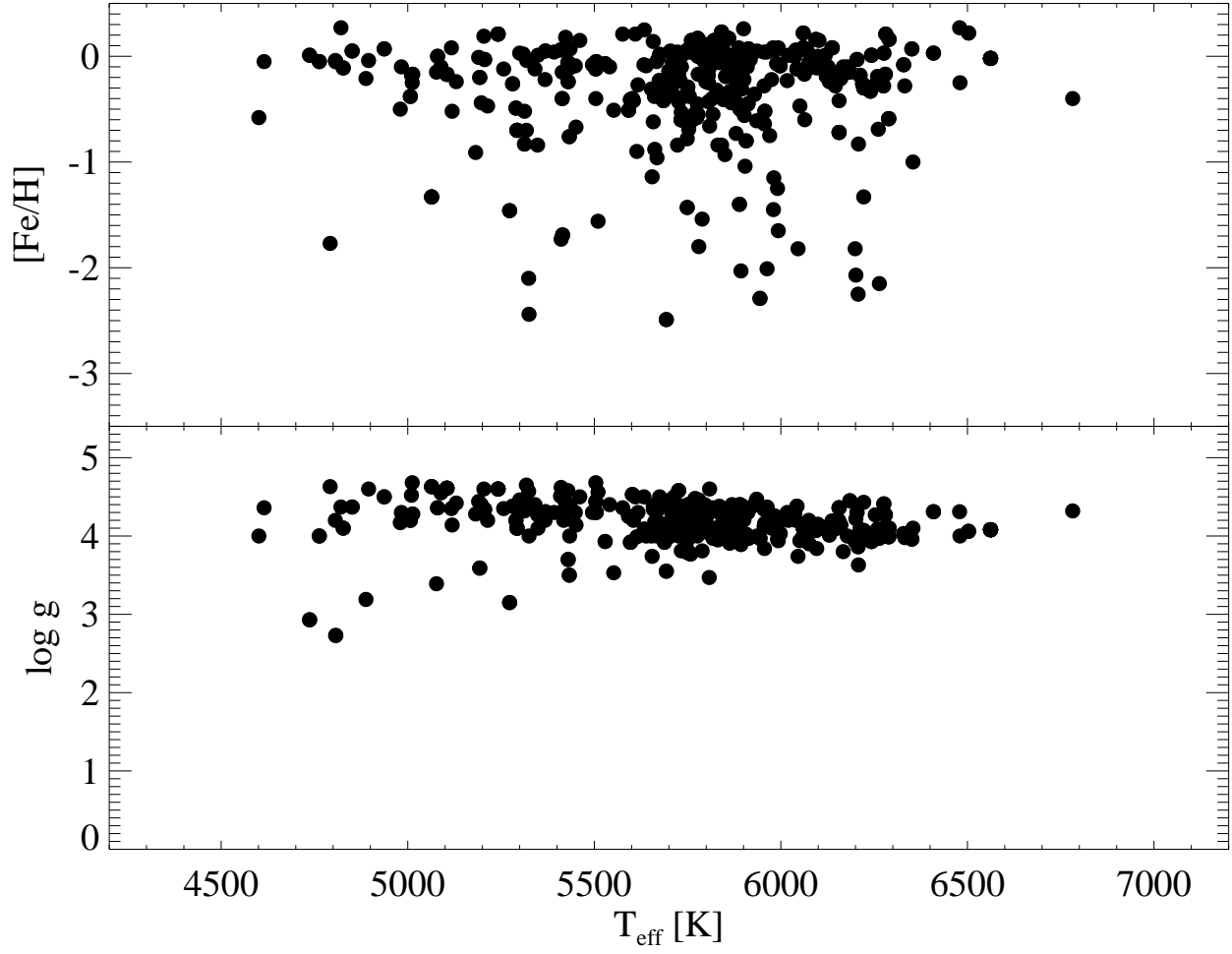


Fig. 3.— Distribution of the stars in the ELODIE sample over  $T_{\text{eff}}$ ,  $\log g$ , and  $[\text{Fe}/\text{H}]$  parameter space.

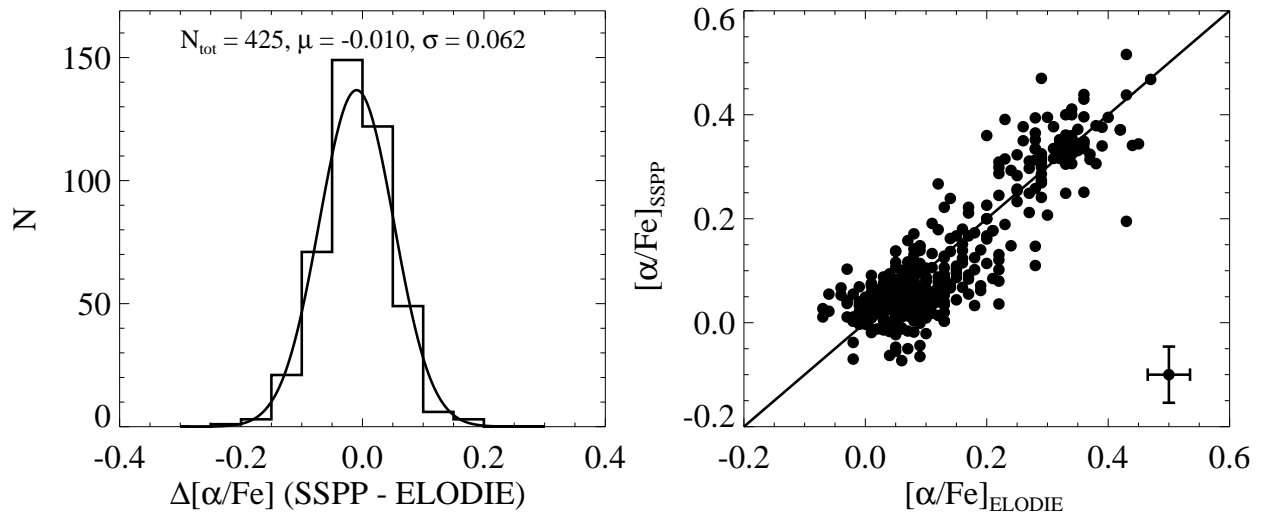


Fig. 4.— Comparisons of  $[\alpha/\text{Fe}]$  obtained from our estimates (SSPP) with 425 selected spectra from the ELODIE sample. The left-hand panel shows a Gaussian fit to the residuals between  $[\alpha/\text{Fe}]$  for our method and values calculated from the literature, while the right-hand panel is a run of our determination of  $[\alpha/\text{Fe}]$  against the values for the ELODIE spectra. The black line in the right-hand panel is the perfect correlation line. In this panel, individual error bars are suppressed for clarity. Instead, a typical error bar is shown in the lower-right corner.

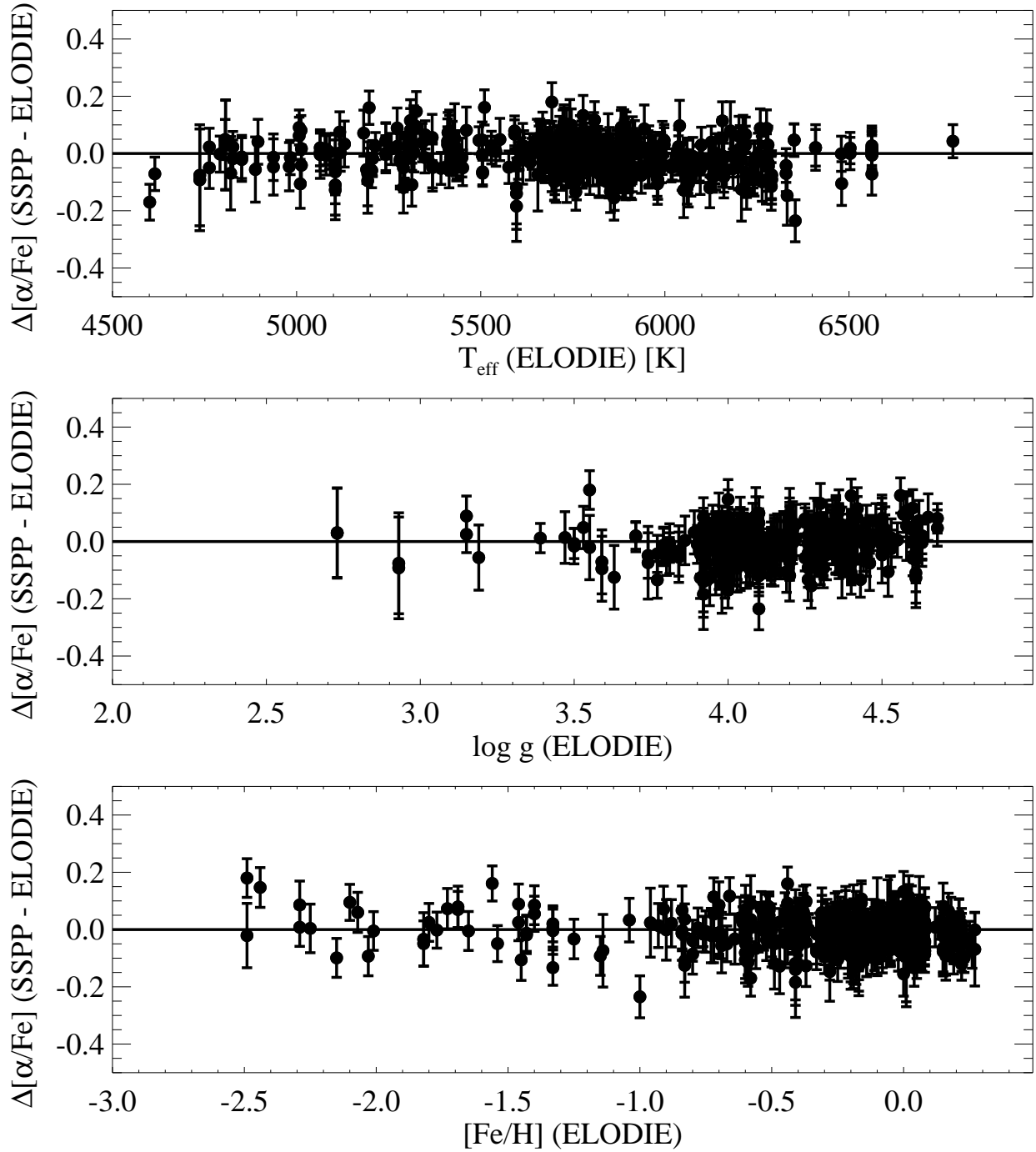


Fig. 5.— Variations in  $[\alpha/\text{Fe}]$  as functions of  $T_{\text{eff}}$ ,  $\log g$ , and  $[\text{Fe}/\text{H}]$ , from upper to lower panels, respectively, for the ELODIE spectra. Quadratically added vertical error bars are shown. There appears to be little or no covariance in the determined  $[\alpha/\text{Fe}]$  along with various ranges for each parameter.

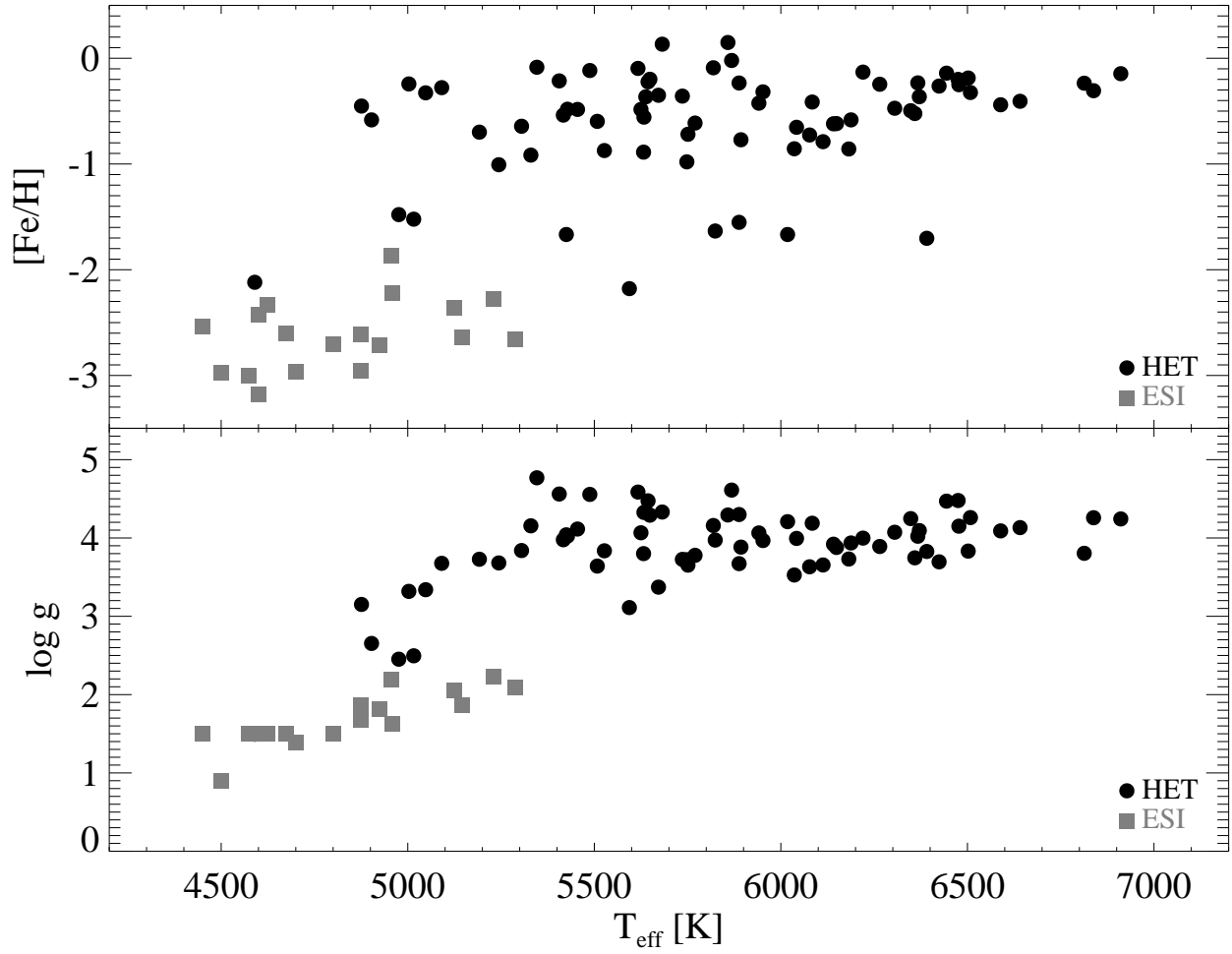


Fig. 6.— Distribution of the stars with the high-resolution spectra over  $T_{\text{eff}}$ ,  $\log g$ , and  $[\text{Fe}/\text{H}]$  parameter space. The black dots are the HET spectra, while the gray squares are the ESI spectra.

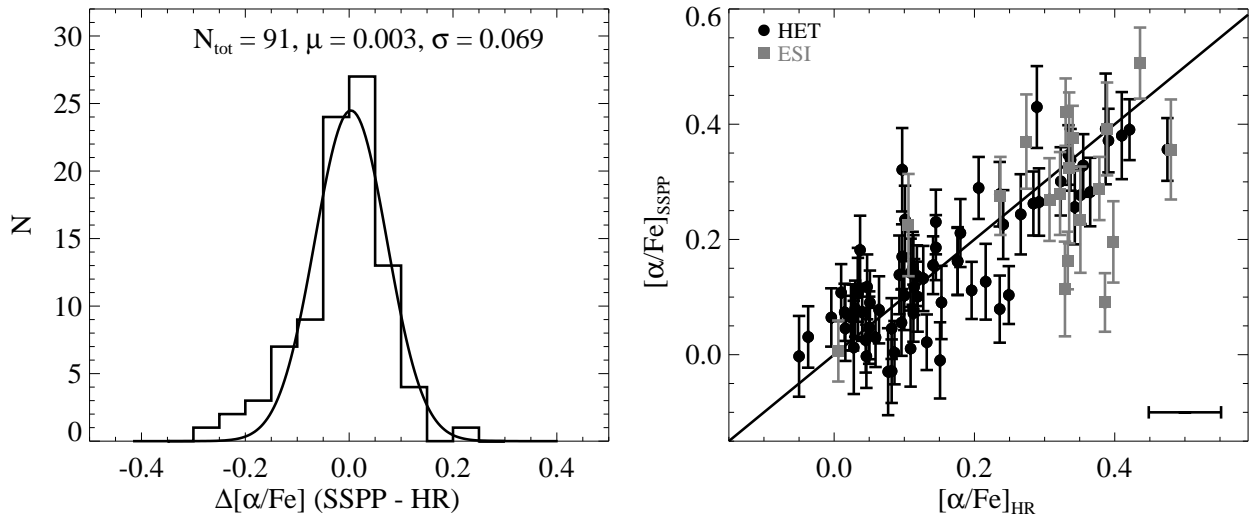


Fig. 7.— Comparisons of  $[\alpha/\text{Fe}]$  from our estimates (SSPP) for 91 stars having either HET (black dots) or ESI (gray squares) high-resolution analyses (collectively referred to as HR). The left-hand panel shows a Gaussian fit to the residuals between  $[\alpha/\text{Fe}]$  for our method and the HR analyses, whereas the right-hand panel displays our determination of  $[\alpha/\text{Fe}]$  vs. the values for the HR analyses. The solid line is the one-to-one line. For clarity, only a typical HR error bar is shown in the lower-right corner.

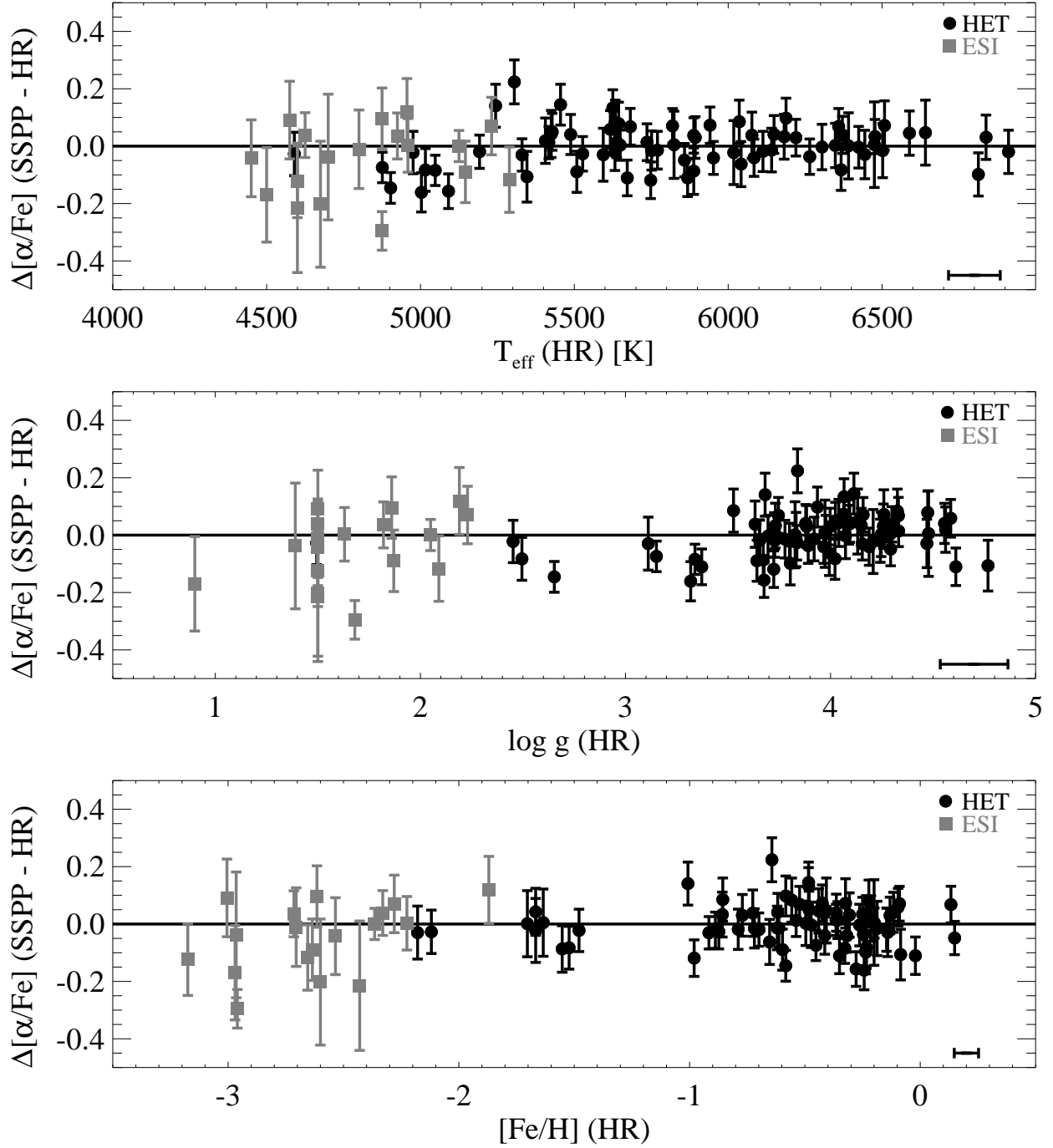


Fig. 8.— Variations in  $[\alpha/\text{Fe}]$  as functions of  $T_{\text{eff}}$ ,  $\log g$ , and  $[\text{Fe}/\text{H}]$ , from upper to lower panel, respectively, for the SDSS/SEGUE high-resolution spectra. The black dots are the HET spectra, and the gray squares are the ESI spectra. Quadratically-added vertical error bars are shown, and a typical error bar on each parameter from the high-resolution analysis is displayed in the lower-right corner of each panel. There appears to be little or no covariance in the determined  $[\alpha/\text{Fe}]$  along with various ranges of each parameter.

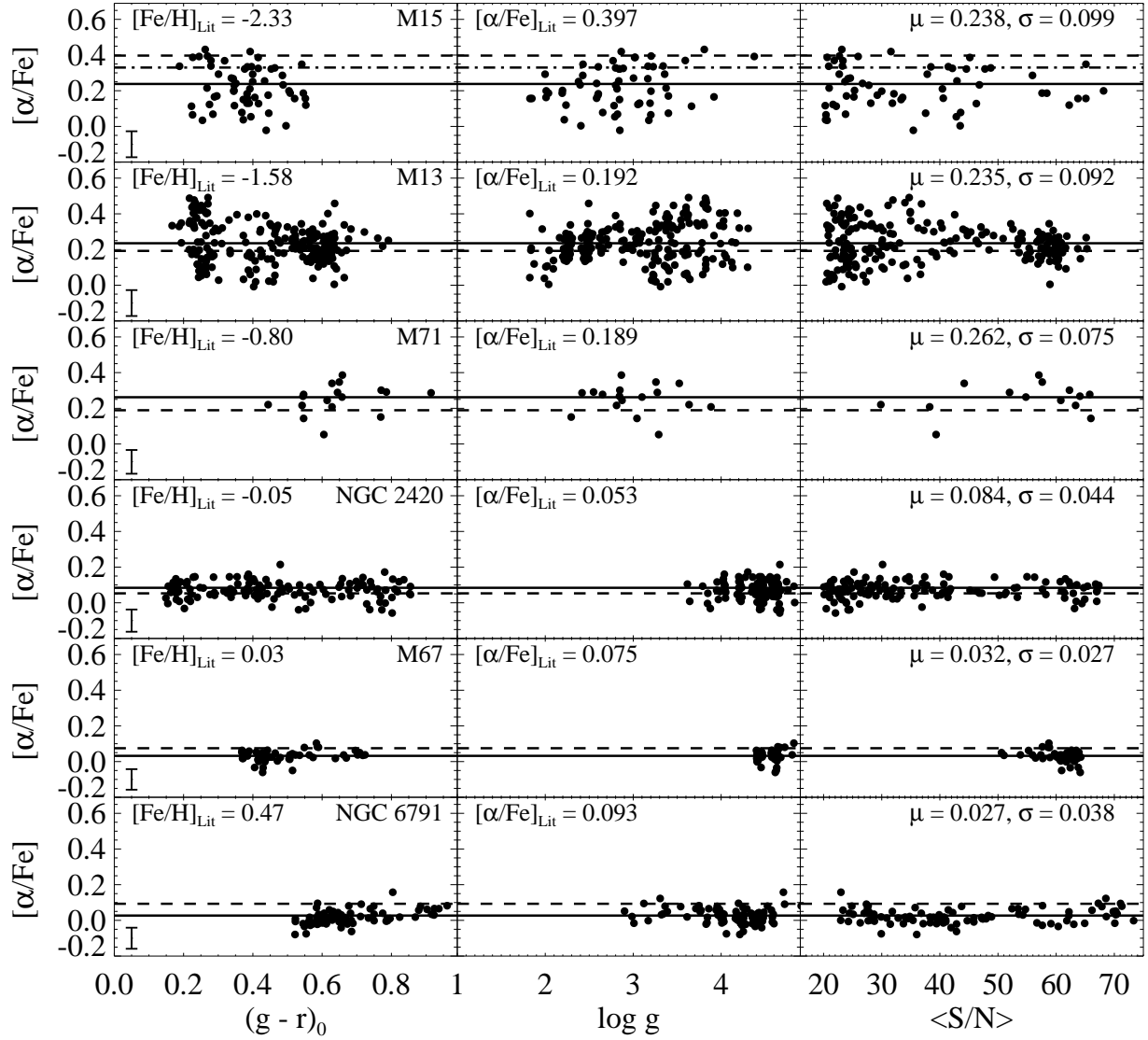


Fig. 9.— Distribution of our measured  $[\alpha/\text{Fe}]$  for likely member stars of M15, M13, M71, NGC 2420, M67, and NGC 6791 from upper to lower panels respectively, as functions of  $(g-r)_0$ ,  $\log g$ , and  $\langle S/N \rangle$ , the average signal-to-noise ratio per pixel. The solid line is the weighted mean of our estimated  $[\alpha/\text{Fe}]$  for the likely members for each cluster, while the dashed line is a weighted average of reported literature values for  $\alpha$ -elements in each cluster (see the text). A typical error bar in  $[\alpha/\text{Fe}]$  for each cluster is shown in the left-hand panels. With the exception of M15, our  $[\alpha/\text{Fe}]$  estimates agree with the averaged literature values within the star-to-star scatter among the likely member stars. The literature determination of  $[\alpha/\text{Fe}]$  for M15 may be problematic (see the text). The dash-dotted line shown for this cluster, which appears to be in better agreement with our determination, within the star-to-star scatter, is the average of  $[\alpha/\text{Fe}]$  derived by Kirby et al. (2008a) using medium-resolution ( $R = 6000$ ) spectra of member stars in M15. Inspection of these panels reveals little or no significant trends in  $[\alpha/\text{Fe}]$  determinations for these clusters as a function of color, surface gravity, or signal-to-noise ratio. However, the error in the measured  $[\alpha/\text{Fe}]$  seems to increase as both  $[\text{Fe}/\text{H}]$  and  $\langle S/N \rangle$  decrease.

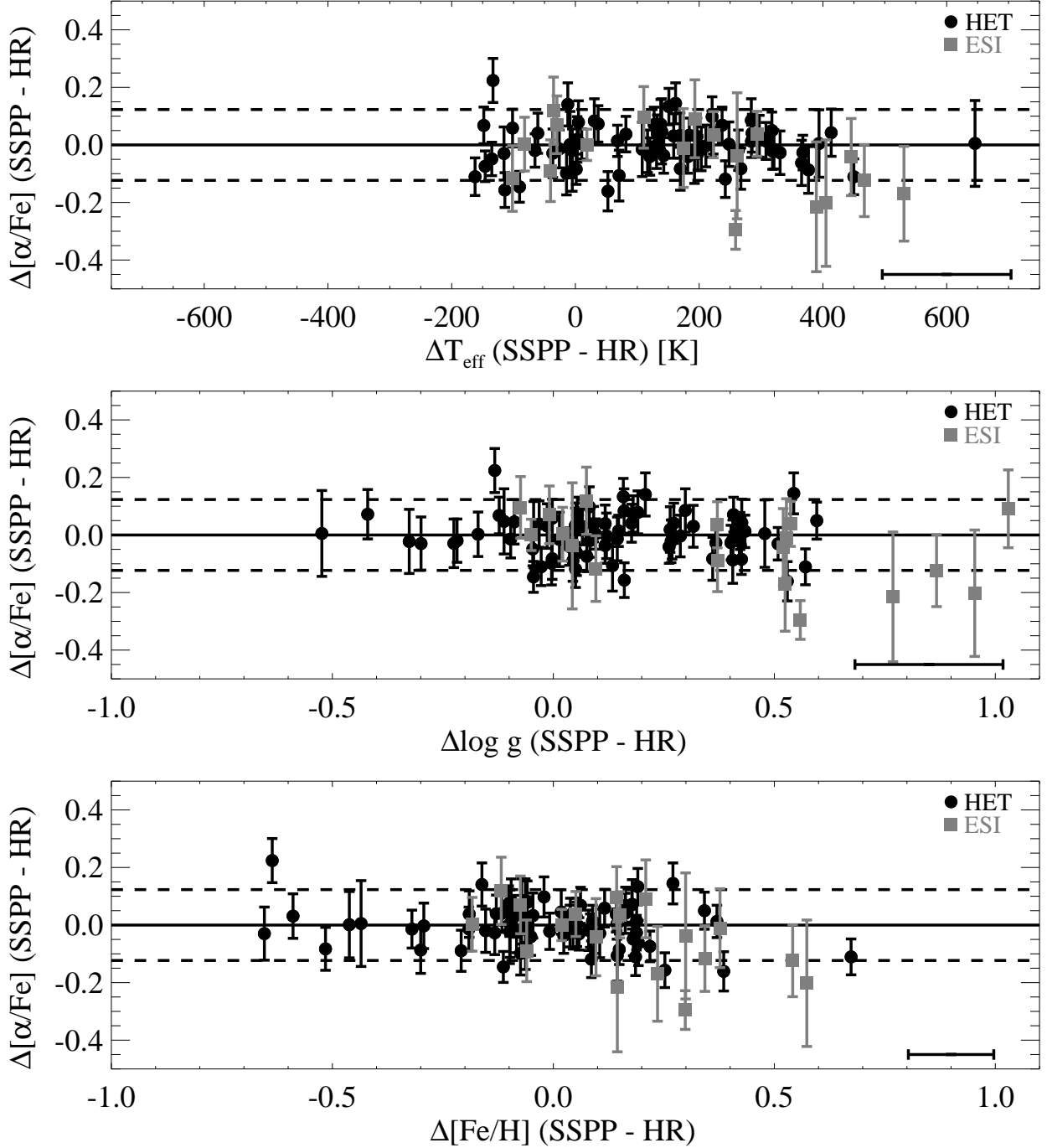


Fig. 10.— Variations in  $[\alpha/\text{Fe}]$  as functions of the residuals in  $T_{\text{eff}}$ ,  $\log g$ , and  $[\text{Fe}/\text{H}]$ , from the upper to lower panels, respectively, between our analysis and the high-resolution analyses. The black dots are the HET spectra, and the gray squares are the ESI spectra. The dashed lines are  $\pm 2\sigma_{\text{tot}}$  ( $\sigma_{\text{tot}} = 0.062$  dex) derived in Section 3.2. Generally, it appears that differences in the  $[\alpha/\text{Fe}]$  estimates for the stars are mostly well within  $\pm 3\sigma_{\text{tot}}$  and that if our estimates of  $T_{\text{eff}}$ ,  $\log g$ , and  $[\text{Fe}/\text{H}]$  are higher, the determined  $[\alpha/\text{Fe}]$  is slightly lower than that of the high-resolution analysis results.

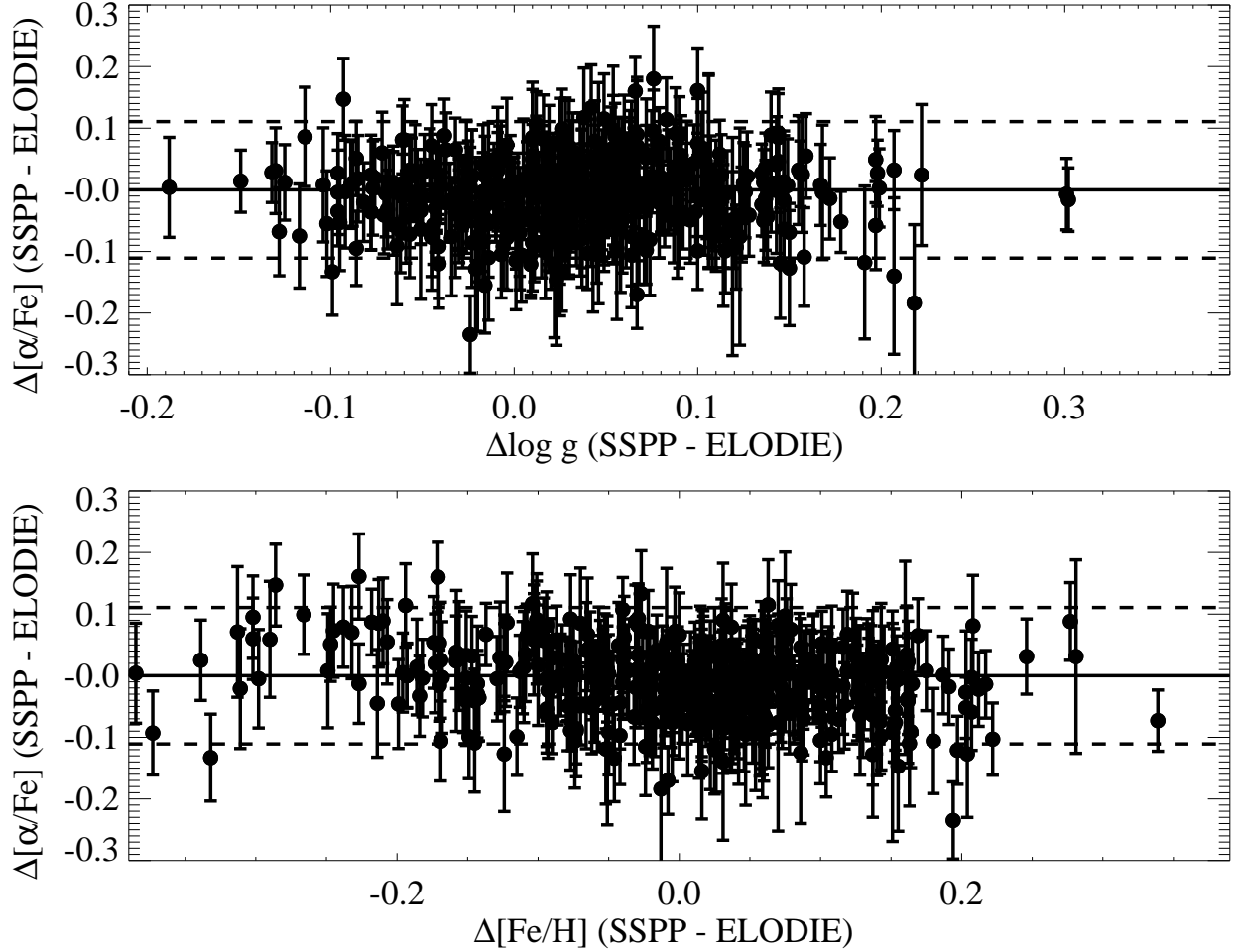


Fig. 11.— Same as shown for Figure 10, but for the ELODIE spectra. The dashed lines are  $\pm 2\sigma_{\text{tot}}$  ( $\sigma_{\text{tot}} = 0.054$  dex) derived in Section 3.1. Note that there is no plot for  $\alpha$ -abundance residuals as a function of  $T_{\text{eff}}$ , since we make use of that value adopted from the literature (see the text). It is noticed that differences in the determined  $[\alpha/\text{Fe}]$  for the stars are mostly inside  $\pm 3\sigma_{\text{tot}}$ .

## REFERENCES

- Abazajian, K., et al. 2003, *AJ*, 126, 2081
- Abazajian, K., et al. 2004, *AJ*, 128, 502
- Abazajian, K., et al. 2005, *AJ*, 129, 1755
- Abazajian, K., et al. 2009, *ApJS*, 182, 543
- Adelman-McCarthy, J. K., et al. 2006, *ApJS*, 162, 38
- Adelman-McCarthy, J. K., et al. 2007, *ApJS*, 172, 634
- Adelman-McCarthy, J. K., et al. 2008, *ApJS*, 175, 297
- Allende Prieto, C. 2006, arXiv:astro-ph/0612200
- Allende Prieto, C., Beers, T. C., Wilhelm, R., Newberg, H. J., Rockosi, C. M., Yanny, B., & Lee, Y. S. 2006, *ApJ*, 636, 804
- Allende Prieto, C., et al. 2008, *AJ*, 136, 2070 (Paper III)
- Alvarez, R., & Plez, B. 1998, *A&A*, 330, 1109
- Anthony-Twarog, B. J., Tanner, D., Cracraft, M., & Twarog, B. A. 2006, *AJ*, 131, 461
- Asplund, M., Grevesse, N., & Sauval, A. J. 2005, in *ASP Conf. Ser. 336, Cosmic Abundances as Records of Stellar Evolution and Nucleosynthesis*, ed. T. G. Barnes, III & F. N. Bash (San Francisco, CA: ASP), 25
- Bailer-Jones, C. A. L. 2000, *A&A*, 357, 197
- Barklem, P. S., & O'Mara, B. J. 1998, *MNRAS*, 300, 863
- Beers, T. C., Rossi, S., Norris, J. E., Ryan, S. G., & Shefler, T. 1999, *ApJ*, 117, 981
- Belokurov, V., et al. 2006, *ApJ*, 647, L111
- Belokurov, V., et al. 2007, *ApJ*, 654, 897
- Belokurov, V., et al. 2008, *ApJ*, 686, L83
- Belokurov, V., et al. 2010, *ApJ*, 712, L103
- Bensby, T., Feltzing, S., & Lundström, I. 2003, *A&A*, 410, 527

- Bensby, T., Feltzing, S., Lundström, I., & Ilyin, I. 2005, *A&A*, 433, 185
- Boesgaard, A. M., King, J. R., Cody, A. M., Stephens, A., & Deliyannis, C. P. 2005, *ApJ*, 629, 832
- Carollo, D., et al. 2007, *Nature*, 450, 1020
- Carollo, D., et al. 2010, *ApJ*, 712, 692
- Carretta, E., Bragaglia, A., & Gratton, R. G. 2007, *A&A*, 473, 129
- Carretta, E., et al. 2009a, *A&A*, 505, 117
- Carretta, E., Bragaglia, A., Gratton, R., & Lucatello, S. 2009b, *A&A*, 505, 139
- Carretta, E., Bragaglia, A., Gratton, R., D’Orazi, V., & Lucatello, S. 2009c, *A&A*, 508, 695
- Castelli, F., Gratton, R. G., & Kurucz, R. L. 1997, *A&A*, 318, 841
- Castelli, F., & Kurucz, R. L. 2003, in *IAU Symp. 210, Modelling of Stellar Atmospheres*, ed. N. Piskunov, W. W. Weiss, & D. F. Gray (San Francisco: ASP), poster A20 (arXiv:astro-ph/0405087)
- Cenarro, A. J., Cardiel, N., Gorgas, J., Peletier, R. F., Vazdekis, A., & Prada, F. 2001a, *MNRAS*, 326, 959
- Cenarro, A. J., Gorgas, J., Cardiel, N., Pedraz, S., Peletier, R. F., & Vazdekis, A. 2001b, *MNRAS*, 326, 981
- Cohen, J. G., & Meléndez, J. 2005, *AJ*, 129, 303
- Cohen, J. G., Briley, M. M., & Stetson, P. B. 2005, *AJ*, 130, 1177
- Frebel, A., Simon, J. D., Geha, M., & Willman, B. 2010, *ApJ*, 708, 560
- Friel, E. D., & Janes, K. A. 1993, *A&A*, 267, 75
- Friel, E. D., Janes, K. A., Tavares, M., Scott, J., Katsanis, R., Lotz, J., Hong, L., & Miller, N. 2002, *AJ*, 124, 2693
- Fukugita, M., Ichikawa, T., Gunn, J. E., Doi, M., Shimasaku, K., & Schneider, D. P. 1996, *AJ*, 111, 1748
- Fulbright, J. P. 2002, *AJ*, 123, 404
- Geisler, D., Smith, V. V., Wallerstein, G., Gonzalez, G., & Charbonnel, C. 2005, *AJ*, 129, 1428

- Grevesse, N., & Sauval, A. J. 1998, *Space Sci. Rev.*, 85, 161
- Gunn, J. E., et al. 1998, *AJ*, 116, 3040
- Gunn, J. E., et al. 2006, *AJ*, 131, 2332
- Gustafsson, B. 1998, *Space Sci. Rev.*, 85, 419
- Johnson, C. I., Kraft, R. P., Pilachowski, C. A., Sneden, C., Ivans, I. I., & Benman, G. 2005, *PASP*, 117, 1308
- Kirby, E. N., Guhathakurta, P., & Sneden, C. 2008a, *ApJ*, 682, 1217
- Kirby, E. N., Simon, J. D., Geha, M., Guhathakurta, P., & Frebel, A. 2008b, *ApJ*, 685, L43
- Kirby, E. N., Guhathakurta, P., Bolte, M., Sneden, C., & Geha, M. C. 2009, *ApJ*, 705, 328
- Kupka, F., Piskunov, N., Ryabchikova, T. A., Stempels, H. C., & Weiss, W. W. 1999, *A&AS*, 138, 119
- Lai, D. K., Rockosi, C. M., Bolte, M., Johnson, J. A., Beers, T. C., Lee, Y. S., Allende Prieto, C., Yanny, B. 2009, *ApJ*, 697, L63
- Lee, Y. S., et al. 2008a, *AJ*, 136, 2022 (Paper I)
- Lee, Y. S., et al. 2008b, *AJ*, 136, 2050 (Paper II)
- Matteucci, F., & Recchi, S. 2001, *ApJ*, 558, 351
- McWilliam, A. 1997, *ARA&A*, 35, 503
- Morrison, H. L., et al. 2003, *AJ*, 125, 2502
- Moultaka, J., Ilovaisky, S. A., Prugniel, P., & Soubiran, C. 2004, *PASP*, 116, 693
- Nelder, J., & Mead, R. 1965, *Computer Journal*, 7, 308
- Nomoto, K., Thielemann, F. -K., & Wheeler, C. J. 1984, *ApJ*, 279, L23
- Pancino, E., Carrera, R., Rossetti, E., & Gallart, C. 2010, *A&A*, 511, 56
- Pier, J. R., Munn, J. A., Hindsley, R. B., Hennessy, G. S., Kent, S. M., Lupton, R. H., Ivezić, Ž. 2003, *AJ*, 125, 1559
- Plez, B., & Cohen, J. G. 2005, *A&A*, 434, 1117

- Ramsey, L. W., et al. 1998, Proc. SPIE, 3352, 34
- Randich, S., Sestito, P., Primas, F., Pallavicini, R., & Pasquini, L. 2006, A&A, 450, 557
- Reddy, B. E., Lambert, D. L., & Allende Prieto, C. 2006, MNRAS, 367, 1329
- Re Fiorentin, P., Bailer-Jones, C. A. L., Lee, Y. S., Beers, T. C., Sivarani, T., Wilhelm, R., Allende Prieto, C., & Norris, J. E. 2007, A&A, 467, 1373
- Shetrone, M., Côté, P., & Sargent, W. L. W. 2001, ApJ, 548, 592
- Shetrone, M., Venn, K. A., Tolstoy, E., Primas, F., Hill, V., & Kaufer, A. 2003, AJ, 125, 684
- Sheinis, A. I., Bolte, M., Epps, H. W., Kibrick, R. I., Miller, J. S., Radovan, M. V., Bigelow, B. C., & Sutin, B. M. 2002, PASP, 114, 851
- Smolinski, J., et al. 2010, AJ, submitted (arXiv:1008.1959; Paper IV)
- Snedden, C., Kraft, R. P., Shetrone, M. D., Smith, G. H., Langer, G. E., & Prosser, C. F. 1997, AJ, 114, 1964
- Snedden, C., Pilachowski, C. A., & Kraft, R. P. 2000, AJ, 120, 1351
- Snedden, C., Kraft, R. P., Guhathakurta, P., Peterson, R. C., & Fulbright, J. P. 2004, AJ, 127, 2162
- Steinmetz, M., et al. 2006, AJ, 132, 1645
- Stoughton, C., et al. 2002, AJ, 123, 485
- Timmes, F., Woosley, S. E., & Weaver, T. A. 1995, ApJS, 98, 617
- Tinsley, B. M. 1979 ApJ, 229, 1046
- Tolstoy, E., Venn, K. A., Shetrone, M., Primas, F., Hill, V., Kaufer, A., & Szeifert, T. 2003, AJ, 125, 707
- Tull, R. G. 1998, Proc. SPIE, 3355, 387
- Unavane, M., Wyse, R. F. G., & Gilmore, G. 1996, MNRAS, 278, 727
- Venn, K. A., Irwin, M., Shetrone, M. D., Tout, C. A., Hill, V., & Tolstoy, E. 2004, AJ, 128, 1177
- Willemsen, P. G., Hilker, M., Kayser, A., & Bailer-Jones, C. A. L. 2005, A&A, 436, 379
- Yanny et al. 2009, AJ, 137, 4377

Yong, D., Carney, B. W., & Teixeira de Almeida, M. L. 2005, *AJ*, 130, 597

York, D. G., et al. 2000, *AJ*, 120, 1579

Zucker, D. B., et al. 2006a, *ApJ*, 650, L41

Zucker, D. B., et al. 2006b, *ApJ*, 643, L103

Zwitter, T., et al. 2008, *AJ*, 136, 421